2. Nuclear models and stability

The aim of this chapter is to understand how certain combinations of N neutrons and Z protons form bound states and to understand the masses, spins and parities of those states. The known (N, Z) combinations are shown in Fig. 2.1. The great majority of nuclear species contain excess neutrons or protons and are therefore β-unstable. Many heavy nuclei decay by α-particle emission or by other forms of spontaneous fission into lighter elements. Another aim of this chapter is to understand why certain nuclei are stable against these decays and what determines the dominant decay modes of unstable nuclei. Finally, forbidden combinations of (N, Z) are those outside the lines in Fig. 2.1 marked "last proton/neutron unbound." Such nuclei rapidly (within $\sim 10^{-20}$s) shed neutrons or protons until they reach a bound configuration.

The problem of calculating the energies, spins and parities of nuclei is one of the most difficult problems of theoretical physics. To the extent that nuclei can be considered as bound states of nucleons (rather than of quarks and gluons), one can start with empirically established two-nucleon potentials (Fig. 1.12) and then, in principle, calculate the eigenstates and energies of many nucleon systems. In practice, the problem is intractable because the number of nucleons in a nucleus with $A > 3$ is much too large to perform a direct calculation but is too small to use the techniques of statistical mechanics. We also note that it is sometimes suggested that intrinsic *three-body* forces are necessary to explain the details of nuclear binding.

However, if we put together all the empirical information we have learned, it is possible to construct efficient *phenomenological models* for nuclear structure. This chapter provides an introduction to the characteristics and physical content to the simplest models. This will lead us to a fairly good explanation of nuclear binding energies and to a general view of the stability of nuclear structures.

Much can be understood about nuclei by supposing that, inside the nucleus, individual nucleons move in a potential well defined by the mean interaction with the other nucleons. We therefore start in Sect. 2.1 with a brief discussion of the *mean potential model* and derive some important conclusions about the relative binding energies of different isobars. To complement the mean potential model, in Sect. 2.2 we will introduce the liquid-drop model that treats the nucleus as a semi-classical liquid object. When combined with

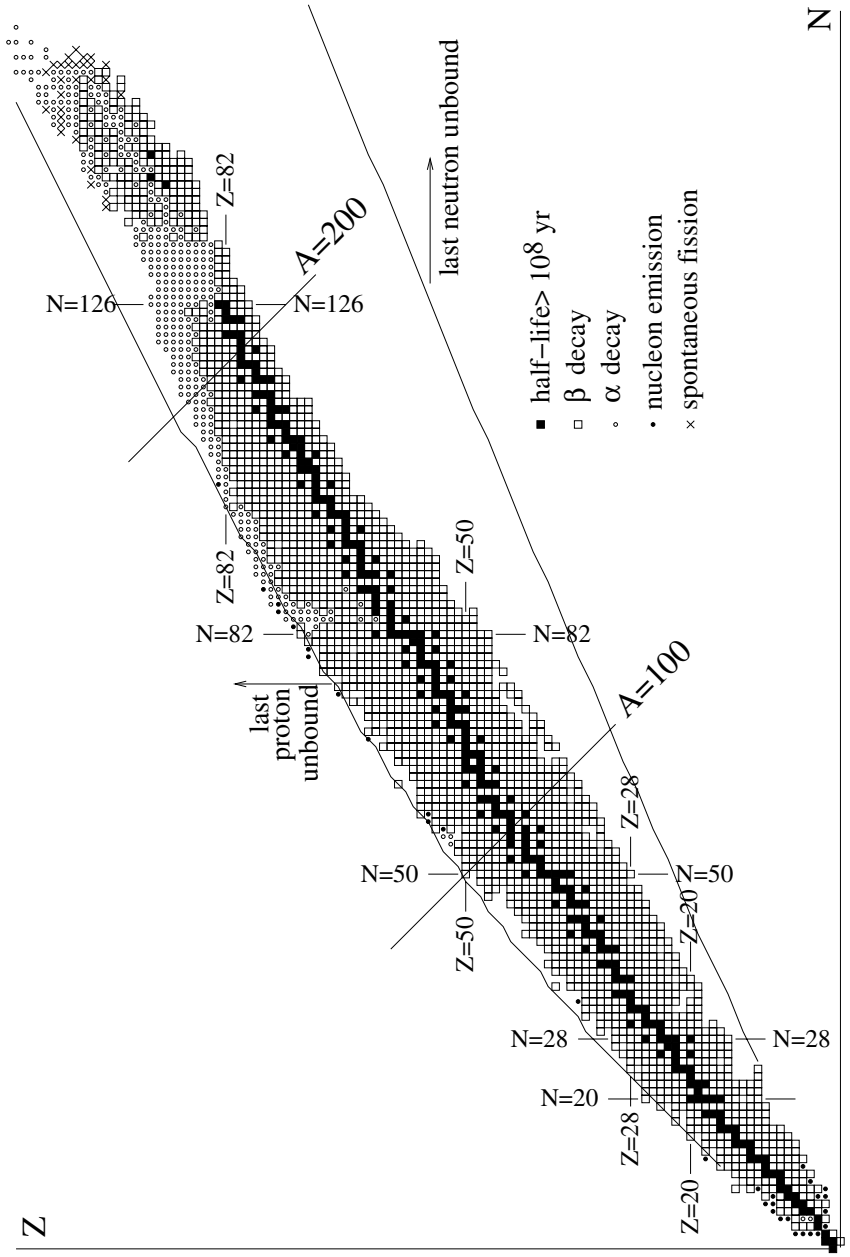

Fig. 2.1. The nuclei. The black squares are long-lived nuclei present on Earth. Combinations of (N, Z) that lie outside the lines marked "last proton/neutron unbound" are predicted to be unbound by the semi-empirical mass formula (2.13). Most other nuclei β-decay or α-decay to long-lived nuclei.

certain conclusions based on the mean potential model, this will allow us to derive Bethe and Weizsäcker's semi-empirical mass formula that gives the binding energy as a function of the neutron number N and proton number Z. In Sect. 2.3 we will come back to the mean potential model in the form of the Fermi-gas model. This model will allow us to calculate some of the parameters in the Bethe–Weizsäcker formula.

In Sect. 2.4 we will further modify the mean-field theory so as to explain the observed nuclear shell structure that lead to certain nuclei with "magic numbers" of neutrons or protons to have especially large binding energies.

Armed with our understanding of nuclear binding, in Sections 2.5 and 2.6 we will identify those nuclei that are observed to be radioactive either via β-decay or α-decay. Finally, in Sect. 2.8, we will discuss attempts to synthesize new metastable nuclei.

2.1 Mean potential model

The *mean potential model* relies on the observation that, to good approximation, individual nucleons behave inside the nucleus as *independent* particles placed in a mean potential (or mean field) due to the other nucleons.

In order to obtain a qualitative description of this mean potential $V(\boldsymbol{r})$, we write it as the sum of potentials $v(\boldsymbol{r}-\boldsymbol{r}')$ between a nucleon at $\boldsymbol{r}$ and a nucleon at $\boldsymbol{r}'$:

$$V(\boldsymbol{r}) = \int v(\boldsymbol{r}-\boldsymbol{r}')\rho(\boldsymbol{r}')d\boldsymbol{r}' \quad . \tag{2.1}$$

In this equation, the nuclear density $\rho(\boldsymbol{r}')$, is proportional to the probability per unit volume to find a nucleus in the vicinity of $\boldsymbol{r}'$. It is precisely that function which we represented on Fig. 1.1 in the case of protons.

We now recall what we know about v and ρ. The strong nuclear interaction $v(\boldsymbol{r}-\boldsymbol{r}')$ is attractive and short range. It falls to zero rapidly at distances larger than $\sim 2\,\mathrm{fm}$, while the typical diameter on a nucleus is "much" bigger, of the order of 6 fm for a light nucleus such as oxygen and of 14 fm for lead. In order to simplify the expression, let us approximate the potential v by a delta function (i.e. a point-like interaction)

$$v(r-r') \sim -v_0\delta(r-r') \quad . \tag{2.2}$$

The constant v_0 can be taken as a free parameter but we would expect that the integral of this potential be the same as that of the original two-nucleon potential (Table 3.3):

$$v_0 \;=\; \int \mathrm{d}^3\boldsymbol{r}\, v(\boldsymbol{r}) \;\sim\; 200\,\mathrm{MeV\,fm}^3 \;, \tag{2.3}$$

where we have used the values from Table 3.3. The mean potential is then simply

$$V(r) = -v_0 \rho(r) \; . \tag{2.4}$$

Using $\rho \sim 0.15\,\mathrm{fm}^{-3}$ we expect to find a potential depth of roughly

$$V(r < R) \;\sim\; -30\,\mathrm{MeV} \; , \tag{2.5}$$

where R is the radius of the nucleus.

The shapes of charge densities in Fig. 1.1 suggest that in first approximation the mean potential has the shape shown in Fig. 2.2a. A much-used analytic expression is the Saxon–Woods potential

$$V(r) = -\frac{V_0}{1 + \exp(r - R)/R} \tag{2.6}$$

where V_0 is a potential depth of the order of 30 to 60 MeV and R is the radius of the nucleus $R \sim 1.2A^{1/3}$ fm. An even simpler potential which leads to qualitatively similar results is the harmonic oscillator potential drawn on Fig. 2.2b:

$$V(r) = -V_0[1 - \left(\frac{r}{R}\right)^2] = -V_0 + \frac{1}{2}M\omega^2 r^2 \qquad r \,<\, R \tag{2.7}$$

with $V_0 = \frac{1}{2}M\omega^2 R^2$, and $V(r > R) = 0$. Contrary to what one could believe from Fig. 2.2, the low-lying wave functions of the two potential wells (a) and (b) are very similar. Quantitatively, their scalar products are of the order of 0.9999 for the ground state and 0.9995 for the first few excited states for an appropriate choice of the parameter ω in b. The first few energy levels of the potentials a and b hardly differ.

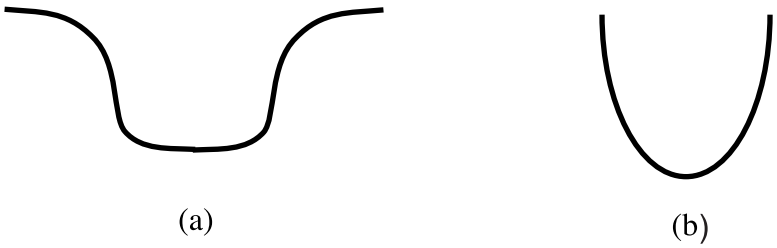

Fig. 2.2. The mean potential and its approximation by a harmonic potential.

In this model, where the nucleons can move independently from one another, and where the protons and the neutrons separately obey the Pauli principle, the energy levels and configurations are obtained in an analogous way to that for complex atoms in the Hartree approximation. As for the electrons in such atoms, the proton and neutron orbitals are independent fermion levels.

It is instructive, for instance, to consider, within the mean potential notion, the stability of various $A = 7$ nuclei, schematically drawn on Fig. 2.3. The figure reminds us that, because of the Pauli principle, nuclei with a large

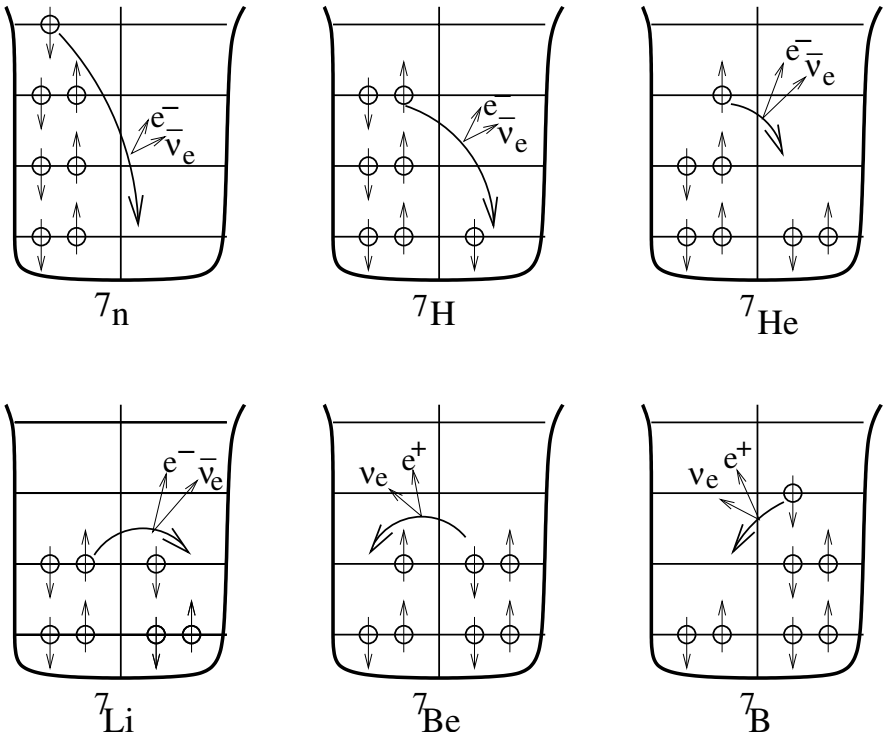

Fig. 2.3. Occupation of the lowest lying levels in the mean potential for various isobars $A = 7$. The level spacings are schematic and do not have realistic positions. The proton orbitals are shown at the same level as the neutron orbitals whereas in reality the electrostatic repulsion raises the protons with respect to the neutrons. The curved arrows show possible neutron–proton and proton–neutron transitions. If energetically possible, a neutron can transform to a proton by emitting a $e^-\bar{\nu}_e$ pair. If energetically possible, a proton can transform to a neutron by emitting a $e^+\nu_e$ pair or by absorbing an atomic e^- and emitting a ν_e. As explained in the text, which of these decays is actually energetically possible depends on the relative alignment of the neutron and proton orbitals.

excess of neutrons over protons or vice versa require placing the nucleons in high-energy levels. This suggests that the lowest energy configuration will be the ones with nearly equal numbers of protons and neutrons, ^{7}Li or ^{7}Be. We expect that the other configurations can β-decay to one of these two nuclei by transforming neutrons to protons or vice versa. The observed masses of the $A = 7$ nuclei, shown in Fig. 2.4, confirm this basic picture:

- The nucleus ^{7}Li is the most bound of all. It is stable, and more strongly bound than its mirror nucleus ^{7}Be which suffers from the larger Coulomb repulsion between the 4 protons. In this nucleus, the actual energy levels of the protons are increased by the Coulomb interaction. The physical

properties of these two nuclei which form an isospin doublet, are very similar.

- The mirror nuclei ^{7}B and ^{7}He can β-decay, respectively, to ^{7}Be and ^{7}Li. In fact, the excess protons or neutrons are placed in levels that are so high that neutron emission is possible for ^{7}He and 3-proton emission for ^{7}B and these are the dominant decay modes. When nucleon emission is possible, the lifetime is generally very short, $\tau \sim 10^{-22}$s for ^{7}B and $\sim 10^{-21}$s for ^{7}He.
- No bound states of ^{7}n, ^{7}H, ^{7}C or ^{7}N have been observed.

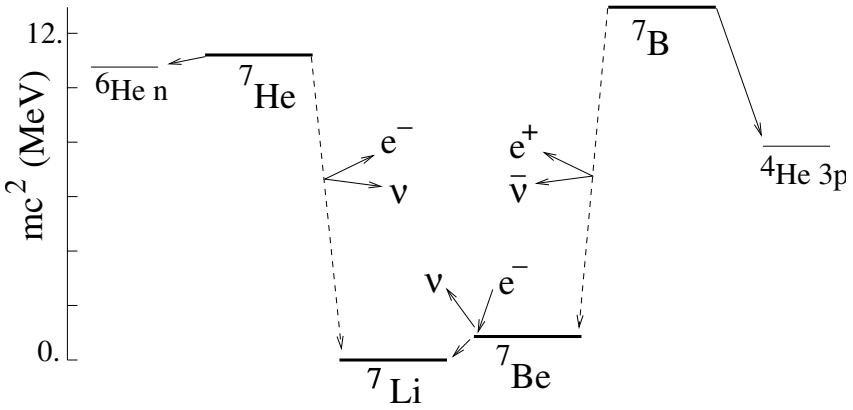

Fig. 2.4. Energies of the $A = 7$ isobars. Also shown are two unbound $A = 7$ states, ^{6}He n and ^{4}He 3p.

This picture of a nucleus formed with independent nuclei in a mean potential allows us to understand several aspects of nuclear phenomenology.

- For a given A, the minimum energy will be attained for optimum numbers of protons and neutrons. If protons were not charged, their levels would be the same as those of neutrons and the optimum would correspond to $N = Z$ (or $Z \pm 1$ for odd A). This is the case for light nuclei, but as A increases, the proton levels are increased compared to the neutron levels owing to Coulomb repulsion, and the optimum combination has $N > Z$. For mirror nuclei, those related by exchanging N and Z, the Coulomb repulsion makes the nucleus $N > Z$ more strongly bound than the nucleus $Z > N$.
- The binding energies are stronger when nucleons can be grouped into pairs of neutrons and pairs of protons with opposite spin. Since the nucleon–nucleon force is attractive, the energy is lowered if nucleons are placed near each other but, according to the Pauli principle, this is possible only if they have opposite spins. There are several manifestations of this pairing

effect. Among the 160 even-A, β-stable nuclei, only the four light nuclei, ^{2}H, ^{6}Li, ^{10}B, ^{14}N, are "odd-odd", the others being all "even-even." [1]

- The Pauli principle explains why *neutrons can be stable in nuclei while free neutrons are unstable.* Possible β-decays of neutrons in ^{7}n, ^{7}H, ^{7}He and ^{7}Li are indicated by the arrows in Fig. 2.3. In order for a neutron to transform into a proton by β-decay, the final proton must find an energy level such that the process $\mathrm{n} \to \mathrm{p e^- \bar{\nu}_e}$ is energetically possible. If all lower levels are occupied, that may be impossible. This is the case for ^{7}Li because the Coulomb interaction raises the proton levels by slightly more than $(m_\mathrm{n} - m_\mathrm{p} - m_\mathrm{e})c^2 = 0.78\,\mathrm{MeV}$. Neutrons can therefore be "stabilized " by the Pauli principle.
- Conversely, in a nucleus a proton can be "destabilized" if the reaction $\mathrm{p} \to \mathrm{n}{+}\mathrm{e^+}\nu_\mathrm{e}$ can occur. This is possible if the proton orbitals are raised, via the Coulomb interaction, by more than $(m_\mathrm{n}{+}m_\mathrm{e}{-}m_\mathrm{p})c^2 = 1.80\,\mathrm{MeV}$ with respect to the neutron orbitals. In the case of ^{7}Li and ^{7}Be shown in Fig. 2.4, the proton levels are raised by an amount between $(m_\mathrm{n} + m_\mathrm{e} - m_\mathrm{p})c^2$ and $(m_\mathrm{n} - m_\mathrm{e} - m_\mathrm{p})c^2$ so that neither nucleus can β-decay. (The *atom* ^{7}Be is unstable because of the electron-capture reaction of an internal electron of the atomic cloud $^7\mathrm{Be\,e^-} \to {}^7\mathrm{Li}\,\nu_\mathrm{e}$.)

We now come back to (2.7) to determine what value should be assigned to the parameter ω so as to reproduce the observed characteristics of nuclei. Equating the two forms in this equation we find

$$\omega(A) \;=\; \left(\frac{2V_0}{M}\right)^{1/2} R^{-1}\,. \tag{2.8}$$

Equation (2.5) suggests that V_0 is independent of A while empirically we know that R is proportional to $A^{1/3}$. Equation (2.8) then tells us that ω is proportional to $A^{-1/3}$. To get the phenomenologically correct value, we take $V_0 = 20\,\mathrm{MeV}$ and $R = 1.12A^{1/3}$ which yields

$$\hbar\omega \;=\; \left(\frac{2V_0}{m_\mathrm{p}c^2}\right)^{1/2} \frac{\hbar c}{R} \;\sim\; 35\,\mathrm{MeV} \,\times\, A^{-1/3}\,. \tag{2.9}$$

We can now calculate the binding energy $B(A = 2N = 2Z)$ in this model. The levels of the three-dimensional harmonic oscillator are $E_n = (n+3/2)\hbar\omega$ with a degeneracy $g_n = (n+1)(n+2)/2$. The levels are filled up to $n = n_\mathrm{max}$ such that

$$A = 4\sum_{n=0}^{n_\mathrm{max}} g_n \sim 2n_\mathrm{max}^3/3 \tag{2.10}$$

i.e. $n_\mathrm{max} \sim (3A/2)^{1/3}$. (This holds for A large; one can work out a simple but clumsy interpolating expression valid for all A's.)

The corresponding energy is

[1] A fifth, ^{180m}Ta has a half-life of 10^{15}yr and can be considered effectively stable.

$$E = -AV_0 + 4\sum_{n=0}^{n_{\max}} g_n(n+3/2)\hbar\omega \sim -AV_0 + \frac{\hbar\omega n_{\max}^4}{2} \ . \tag{2.11}$$

Using the expressions for $\hbar\omega$ and $n_{\max}$ we find

$$\sim -8\,\mathrm{MeV} \times A \tag{2.12}$$

i.e. the canonical binding energy of 8 MeV per nucleon.

2.2 The Liquid-Drop Model

One of the first nuclear models, proposed in 1935 by Bohr, is based on the short range of nuclear forces, together with the additivity of volumes and of binding energies. It is called the *liquid-drop model*.

Nucleons interact strongly with their nearest neighbors, just as molecules do in a drop of water. Therefore, one can attempt to describe their properties by the corresponding quantities, i.e. the radius, the density, the surface tension and the volume energy.

2.2.1 The Bethe–Weizsäcker mass formula

An excellent parametrization of the binding energies of nuclei in their ground state was proposed in 1935 by Bethe and Weizsäcker. This formula relies on the liquid-drop analogy but also incorporates two quantum ingredients we mentioned in the previous section. One is an *asymmetry* energy which tends to favor equal numbers of protons and neutrons. The other is a *pairing* energy which favors configurations where two identical fermions are paired.

The mass formula of Bethe and Weizsäcker is

$$B(A,Z) \ = \ a_{\mathrm{v}}A \ - \ a_{\mathrm{s}}A^{2/3} \ - \ a_{\mathrm{c}}\frac{Z^2}{A^{1/3}} \ - \ a_{\mathrm{a}}\frac{(N-Z)^2}{A} \ + \ \delta(A) \ . \tag{2.13}$$

The coefficients a_i are chosen so as to give a good approximation to the observed binding energies. A good combination is the following:

$$a_{\mathrm{v}} \ = \ 15.753 \text{ MeV}$$

$$a_{\mathrm{s}} \ = \ 17.804 \text{ MeV}$$

$$a_{\mathrm{c}} \ = \ 0.7103 \text{ MeV}$$

$$a_{\mathrm{a}} \ = \ 23.69 \text{ MeV}$$

and

$$\delta(A) = \begin{cases} 33.6A^{-3/4} & \text{if } N \text{ and } Z \text{ are even} \\ -33.6A^{-3/4} & \text{if } N\text{and } Z \text{ are odd} \\ 0 & \text{si } A = N + Z \text{ is odd} \end{cases} .$$

The numerical values of the parameters must be determined empirically (other than a_{c}), but the A and Z dependence of each term reflects simple physical properties.

- The first term is a *volume* term which reflects the nearest-neighbor interactions, and which by itself would lead to a constant binding energy per nucleon $B/A \sim 16$ MeV.
- The term $a_{\rm s}$, which lowers the binding energy, is a *surface* term. Internal nucleons feel isotropic interactions whereas nucleons near the surface of the nucleus feel forces coming only from the inside. Therefore this is a *surface tension* term, proportional to the area $4\pi R^2 \sim A^{2/3}$.
- The term $a_{\rm c}$ is the *Coulomb repulsion* term of protons, proportional to Q^2/R, i.e. $\sim Z^2/A^{1/3}$. This term is calculable. It is smaller than the nuclear terms for small values of Z. It favors a neutron excess over protons.
- Conversely, the *asymmetry* term $a_{\rm a}$ favors symmetry between protons and neutrons (isospin). In the absence of electric forces, $Z = N$ is energetically favorable.
- Finally, the term $\delta(A)$ is a quantum *pairing* term.

The existence of the Coulomb term and the asymmetry term means that for each A there is a nucleus of maximum binding energy found by setting $\partial B/\partial Z = 0$. As we will see below, the maximally bound nucleus has $Z = N = A/2$ for low A where the asymmetry term dominates but the Coulomb term favors $N > Z$ for large A.

The predicted binding energy for the maximally bound nucleus is shown in Fig. 2.5 as a function of A along with the observed binding energies. The figure only shows even–odd nuclei where the pairing term vanishes. The figure also shows the contributions of various terms in the mass formula. We can see that, as A increases, the surface term loses its importance in favor of the Coulomb term. The binding energy has a broad maximum in the neighborhood of $A \sim 56$ which corresponds to the even-Z isotopes of iron and nickel.

Light nuclei can undergo exothermic fusion reactions until they reach the most strongly bound nuclei in the vicinity of $A \sim 56$. These reactions correspond to the various stages of nuclear burning in stars. For large A's, the increasing comparative contribution of the Coulomb term lowers the binding energy. This explains why heavy nuclei can release energy in fission reactions or in α-decay. In practice, this is observed mainly for very heavy nuclei $A > 212$ because lifetimes are in general too large for smaller nuclei.

For the even–odd nuclei, the binding energy follows a parabola in Z for a given A. An example of this is given on Fig. 2.6 for $A = 111$. The minimum of the parabola, i.e. the number of neutrons and protons which corresponds to the maximum binding energy of the nucleus gives the value $Z(A)$ for the most bound isotope :

$$\frac{\partial B}{\partial Z} = 0 \;\Rightarrow\; Z(A) \;=\; \frac{A}{2 + a_{\rm c} A^{2/3}/2a_{\rm a}} \sim \frac{A/2}{1 + 0.0075\ A^{2/3}}\ . \qquad (2.14)$$

This value of Z is close to, but not necessarily equal to the value of Z that gives the stable isobar for a given A. This is because one must also take

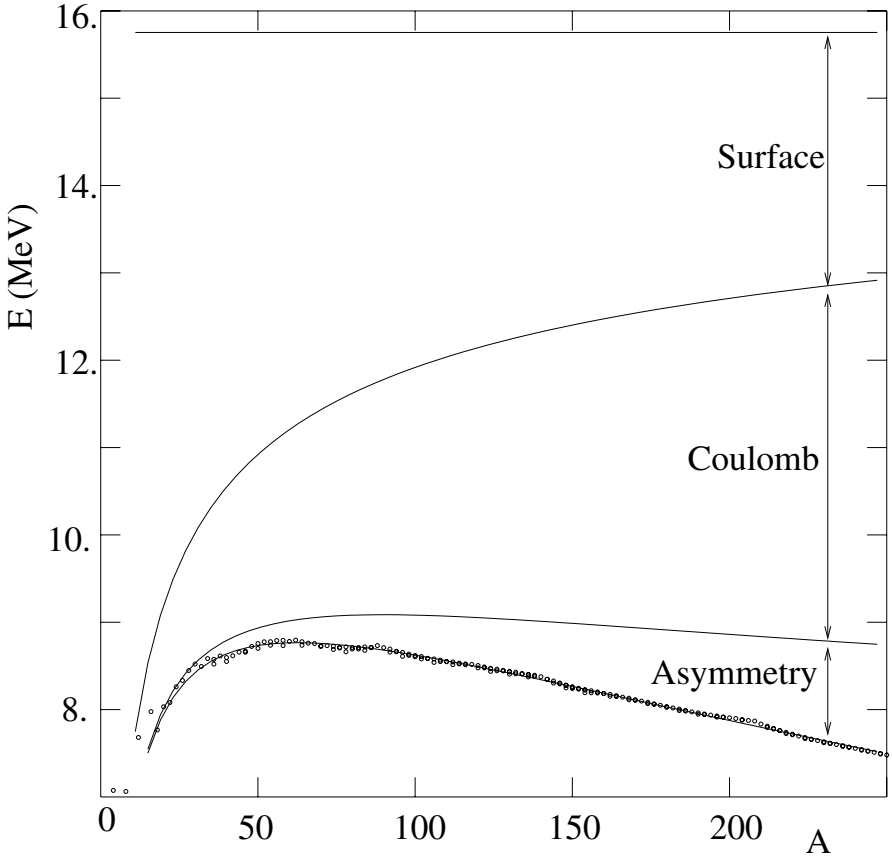

Fig. 2.5. The observed binding energies as a function of A and the predictions of the mass formula (2.13). For each value of A, the most bound value of Z is used corresponding to $Z = A/2$ for light nuclei but $Z < A/2$ for heavy nuclei. Only even–odd combinations of A and Z are considered where the pairing term of the mass formula vanishes. Contributions to the binding energy per nucleon of the various terms in the mass formula are shown.

into account the neutron–proton mass difference in order to make sure of the stability against β-decay. The only stable nuclei for odd A are obtained by minimizing the atomic mass $m(A, Z) + Zm_\mathrm{e}$ (we neglect the binding energies of the atomic electrons). This leads to a slightly different value for the $Z(A)$ of the stable atom:

$$Z(A) \;=\; \frac{(A/2)(1+\delta_\mathrm{npe}/4a_\mathrm{a})}{1+a_\mathrm{c}A^{2/3}/4a_\mathrm{a}} \sim 1.01\,\frac{A/2}{1+0.0075A^{2/3}} \tag{2.15}$$

where $\delta_\mathrm{npe} = m_\mathrm{n} - m_\mathrm{p} - m_\mathrm{e} = 0.75\,\mathrm{MeV}$. This formula shows that light nuclei have a slight preference for protons over neutrons because of their smaller

mass while heavy nuclei have an excess of neutrons over protons because an extra amount of nuclear binding must compensate for the Coulomb repulsion.

For even A, the binding energies follow two parabolas, one for even–even nuclei, the other for odd–odd ones. An example is shown for $A = 112$ on Fig. 2.6. In the case of even–even nuclei, it can happen that an unstable odd-odd nucleus lies between two β-stable even-even isotopes. The more massive of the two β-stable nuclei can decay via 2β-decay to the less massive. The lifetime for this process is generally of order or greater than 10^{20} yr so for practical purposes there are often two stable isobars for even A.

The Bethe–Weizsäcker formula predicts the maximum number of protons for a given N and the maximum number of neutrons for a given Z. The limits are determined by requiring that the last added proton or last added neutron be bound, i.e.

$$B(Z+1,N) - B(Z,N) \; > 0 \; , \qquad B(Z,N+1) - B(Z,N) \; > \; 0 \; , \tag{2.16}$$

or equivalently

$$\frac{\partial B(Z,N)}{\partial Z} \; > \; 0 \; , \qquad \frac{\partial B(Z,N)}{\partial N} \; > \; 0 \; . \tag{2.17}$$

The locus of points (Z, N) where these inequalities become equalities establishes determines the region where bound states exist. The limits predicted by the mass formula are shown in Fig. 2.1. These lines are called the proton and neutron *drip-lines*. As expected, some nuclei just outside the drip-lines are observed to decay rapidly by nucleon emission. Combinations of (Z, N) far outside the drip-lines are not observed. However, we will see in Sect. 2.7 that nucleon emission is observed as a decay mode of many excited nuclear states.

2.3 The Fermi gas model

The Fermi gas model is a quantitative quantum-mechanical application of the mean potential model discussed qualitatively in Sect. 2.1. It allows one to account semi-quantitatively for various terms in the Bethe–Weizsäcker formula. In this model, nuclei are considered to be composed of two fermion gases, a neutron gas and a proton gas. The particles do not interact, but they are confined in a sphere which has the dimension of the nucleus. The interactions appear implicitly through the assumption that the nucleons are confined in the sphere.

The liquid-drop model is based on the saturation of nuclear forces and one relates the energy of the system to its geometric properties. The Fermi model is based on the quantum statistics effects on the energy of confined fermions. The Fermi model provides a means to calculate the constants $a_{\rm v}$, $a_{\rm s}$ and $a_{\rm a}$ in the Bethe–Weizsäcker formula, directly from the density ρ of the nuclear matter. Its semi-quantitative success further justifies for this formula.

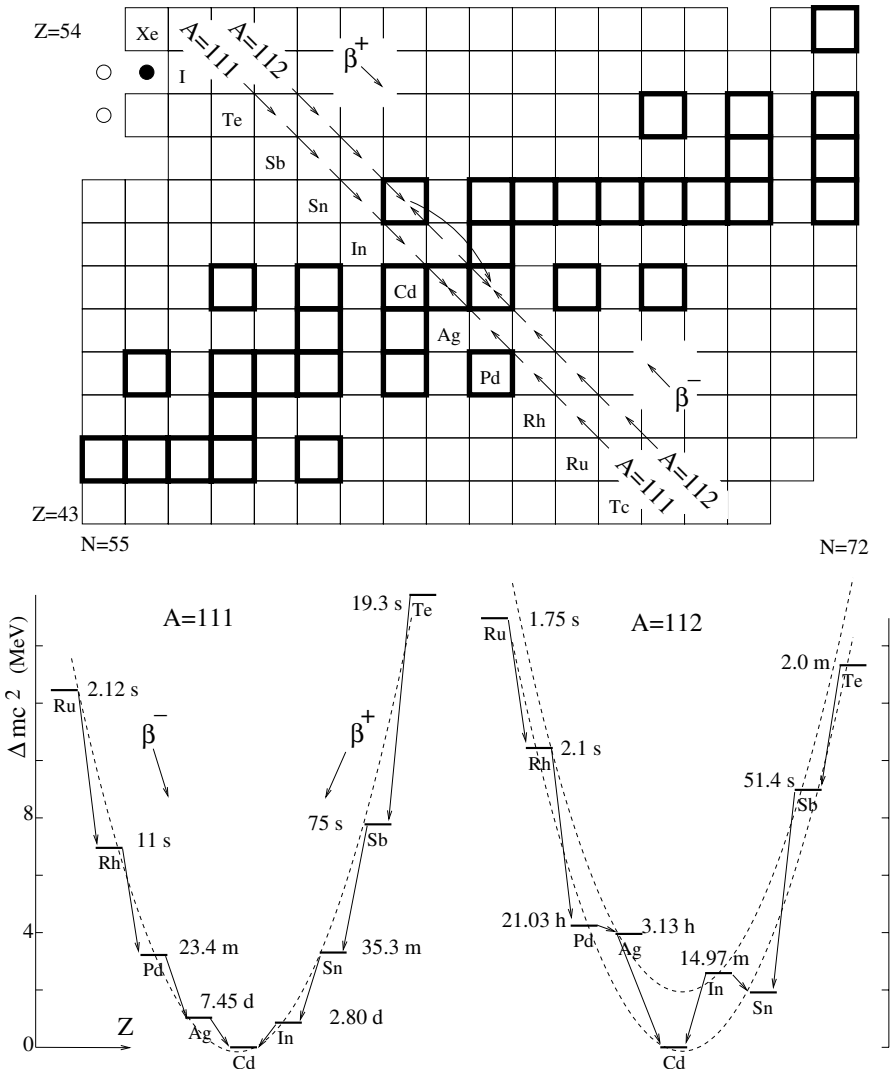

Fig. 2.6. The systematics of β-instability. The top panel shows a zoom of Fig. 2.1 with the β-stable nuclei shown with the heavy outlines. Nuclei with an excess of neutrons (below the β-stable nuclei) decay by β^- emission. Nuclei with an excess of protons (above the β-stable nuclei) decay by β^+ emission or electron capture. The bottom panel shows the atomic masses as a function of Z for $A = 111$ and $A = 112$. The quantity plotted is the difference between $m(Z)$ and the mass of the lightest isobar. The dashed lines show the predictions of the mass formula (2.13) after being offset so as to pass through the lowest mass isobars. Note that for even-A, there can be two β-stable isobars, e.g. ^{112}Sn and ^{112}Cd. The former decays by 2β-decay to the latter. The intermediate nucleus ^{112}In can decay to both.

The Fermi model is based on the fact that a spin 1/2 particle confined to a volume V can only occupy a discrete number of states. In the momentum interval $\mathrm{d}^3\boldsymbol{p}$, the number of states is

$$\mathrm{d}\mathcal{N} = (2s+1)\frac{V\mathrm{d}^3\boldsymbol{p}}{(2\pi\hbar)^3} \quad , \tag{2.18}$$

with $s = 1/2$. This number will be derived below for a cubic container but it is, in fact, generally true. It corresponds to a density in *phase space* of 2 states per $2\pi\hbar^3$ of phase-space volume.

We now place $\mathcal{N}$ particles in the volume. In the ground state, the particles fill up the lowest single-particle levels, i.e. those up to a maximum momentum called the *Fermi momentum*, p_F, corresponding to a maximum energy $\varepsilon_\mathrm{F} = p_\mathrm{F}^2/2m$. The Fermi momentum is determined by

$$\mathcal{N} \;=\; \sum_{p<p_\mathrm{F}} \mathrm{d}\mathcal{N} \;=\; \frac{V\,p_\mathrm{F}^3}{3\pi^2\hbar^3} \quad . \tag{2.19}$$

This determines the Fermi energy

$$\varepsilon_\mathrm{F} \;=\; \frac{p_\mathrm{F}^2}{2m} \;=\; \frac{\hbar^2}{2m}(3\pi^2 n)^{2/3} \tag{2.20}$$

where n is the number density $n = \mathcal{N}/V$. The total (*kinetic*) energy $\mathcal{E}$ of the system is

$$\mathcal{E} \;=\; \sum_{p<p_\mathrm{F}} \frac{p^2}{2m} \;=\; \frac{3}{5}\mathcal{N}\varepsilon_\mathrm{F} \quad . \tag{2.21}$$

In a system of $A = Z + N$ nucleons, the densities of neutrons and protons are respectively $n_0(N/A)$ and $n_0(Z/A)$ where $n_0 \sim 0.15\,\mathrm{fm}^{-3}$ is the nucleon density. The total kinetic energy is then

$$\mathcal{E} = \mathcal{E}_Z + \mathcal{E}_N = 3/5\left[Z\frac{\hbar^2}{2m}(3\pi^2\frac{Zn_0}{A})^{2/3} + N\frac{\hbar^2}{2m}(3\pi^2\frac{Nn_0}{A})^{2/3}\right] . \tag{2.22}$$

In the approximation $Z \sim N \sim A/2$, this value of the nuclear density corresponds to a Fermi energy for protons and neutrons of

$$\varepsilon_\mathrm{F} = 35\ \mathrm{MeV} \quad , \tag{2.23}$$

which corresponds to a momentum and a wave number

$$p_\mathrm{F} = 265\mathrm{MeV}/c\,, \qquad k_\mathrm{F} = p_\mathrm{F}/\hbar = 1.33\,\mathrm{fm}^{-1} \quad . \tag{2.24}$$

2.3.1 Volume and surface energies

In fact, the number of states (2.18) is slightly overestimated since it corresponds to the continuous limit $V \to \infty$ where the energy differences between

levels vanishes. To convince ourselves, we examine the estimation of the number of levels in a cubic box of linear dimension a. The wavefunctions and energy levels are

$$\psi_{n_1,n_2,n_3}(x,y,z) = \sqrt{\frac{8}{a^3}}\ \sin(\frac{n_1\pi x}{a})\ \sin(\frac{n_2\pi y}{a})\ \sin(\frac{n_3\pi z}{a}) \tag{2.25}$$

$$E = E_{n_1,n_2,n_3} = \frac{\hbar^2\pi^2}{2ma^2}(n_1^2+n_2^2+n_3^2) \quad , \tag{2.26}$$

with $n_i > 0$, and one counts the number of states such that $E \leq E_0$, E_0 fixed, which corresponds to the volume of one eighth of a sphere in the space $\{n_1, n_2, n_3\}$. In this counting, one should not take into account the three planes $n_1 = 0$, $n_2 = 0$ and $n_3 = 0$ for which the wavefunction is identically zero, which does not correspond to a physical situation. When the number of states under consideration is very large, such as in statistical mechanics, this correction is negligible. However, it is not negligible here. The corresponding excess in (2.19) can be calculated in an analogous way to (2.18); one obtains

$$\Delta\mathcal{N} = \frac{p_{\rm F}^2\ S}{8\pi\hbar^2} = \frac{m\,\varepsilon_{\rm F}\ S}{4\pi\hbar^2} \tag{2.27}$$

where S is the external area of the volume V ($S = 6\,a^2$ for a cube, $S = 4\pi r_0^2$ for a sphere).[2]

The expression (2.19), after correction for this effect, becomes

$$\mathcal{N} = \frac{V\ p_{\rm F}^3}{3\pi^2\hbar^3} - \frac{S\ p_{\rm F}^2}{4\,\pi\hbar^2} \quad . \tag{2.28}$$

The corresponding energy is

$$\mathcal{E} = \int_0^{p_{\rm F}} \frac{p^2}{2m}\,{\rm d}\mathcal{N}(p) = \frac{V\,\varepsilon_{\rm F} p_{\rm F}^3}{5\pi^2\hbar^2} - \frac{S\,\varepsilon_{\rm F} p_{\rm F}^2}{8\pi\hbar^2} \quad . \tag{2.29}$$

The first term is a volume energy, the second term is a surface correction, or a surface-tension term.

To first order in S/V the kinetic energy per particle is therefore

$$\frac{\mathcal{E}}{\mathcal{N}} = \frac{3}{5}\varepsilon_{\rm F}\,(1 + \frac{\pi\,S\,\hbar}{8V\,p_{\rm F}} + \ldots) \quad . \tag{2.30}$$

In the approximation $Z \sim N \sim A/2$, the kinetic energy is of the form :

$$E_c = a_0 A + a_{\rm s} A^{2/3} \tag{2.31}$$

with

$$a_0 = \frac{3}{5}\varepsilon_{\rm F} = 21\ {\rm MeV}\,, \qquad a_{\rm s} = \frac{3}{5}\varepsilon_{\rm F}\ \frac{3\pi\hbar}{8\,r_0\,p_{\rm F}} = 16.1\,{\rm MeV}\,. \tag{2.32}$$

[2] On can prove that these results, expressed in terms of V and S, are independent of the shape of the confining volume, see R. Balian and C. Bloch, Annals of Physics, **60**, p.40 (1970) and **63**, p.592 (1971).

The second term is the surface coefficient of (2.13), in good agreement with the experimental value. The mean energy per particle is the sum $a_{\rm v} = a_0 - U$ of a_0 and of a potential energy U which can be determined experimentally by neutron scattering on nuclei (this is analogous to the Ramsauer effect). Experiment gives $U \sim -40\,\mathrm{MeV}$, i.e.

$$a_{\rm v} \sim 19\,\mathrm{MeV}\ , \tag{2.33}$$

in reasonable agreement with the empirical value of (2.13).

2.3.2 The asymmetry energy

Consider now the system of the two Fermi gases, with N neutrons and Z protons inside the same sphere of radius R. The total energy of the two gases (2.22) is

$$E = \frac{3}{5}\varepsilon_{\rm F}\left(N(\frac{2N}{A})^{2/3} + Z(\frac{2Z}{A})^{2/3}\right) \quad , \tag{2.34}$$

where we neglect the surface energy. Expanding this expression in the neutron excess $\Delta = N - Z$, we obtain, to first order in Δ/A,

$$E = \frac{3}{5}\varepsilon_{\rm F} + \frac{\varepsilon_{\rm F}}{3}\frac{(N-Z)^2}{A} + \dots\ . \tag{2.35}$$

This is precisely the form of the asymmetry energy in the Bethe–Weizsäcker formula. However, the numerical value of the coefficient $a_{\rm a} \sim 12$ MeV is half of the empirical value. This defect comes from the fact that the Fermi model is too simple and does not contain enough details about the nuclear interaction.

2.4 The shell model and magic numbers

In atomic physics, the ionization energy E_I, i.e. the energy needed to extract an electron from a neutral atom with Z electrons, displays discontinuities around $Z = 2, 10, 18, 36, 54$ and 86, i.e. for noble gases. These discontinuities are associated with closed electron shells.

An analogous phenomenon occurs in nuclear physics. There exist many experimental indications showing that atomic nuclei possess a shell-structure and that they can be constructed, like atoms, by filling successive shells of an effective potential well. For example, the nuclear analogs of atomic ionization energies are the "separation energies" $S_{\rm n}$ and $S_{\rm p}$ which are necessary in order to extract a neutron or a proton from a nucleus

$$S_{\rm n} = B(Z,N) - B(Z,N-1) \quad S_{\rm p} = B(Z,N) - B(Z-1,N)\ . \tag{2.36}$$

These two quantities present discontinuities at special values of N or Z, which are called *magic numbers*. The most commonly mentioned are:

$$2\ \ 8\ \ 20\ \ 28\ \ 50\ \ 82\ \ 126\,. \tag{2.37}$$

As an example, Fig. 2.7 gives the neutron separation energy of lead isotopes ($Z = 82$) as a function of N. The discontinuity at the magic number $N = 126$ is clearly seen.

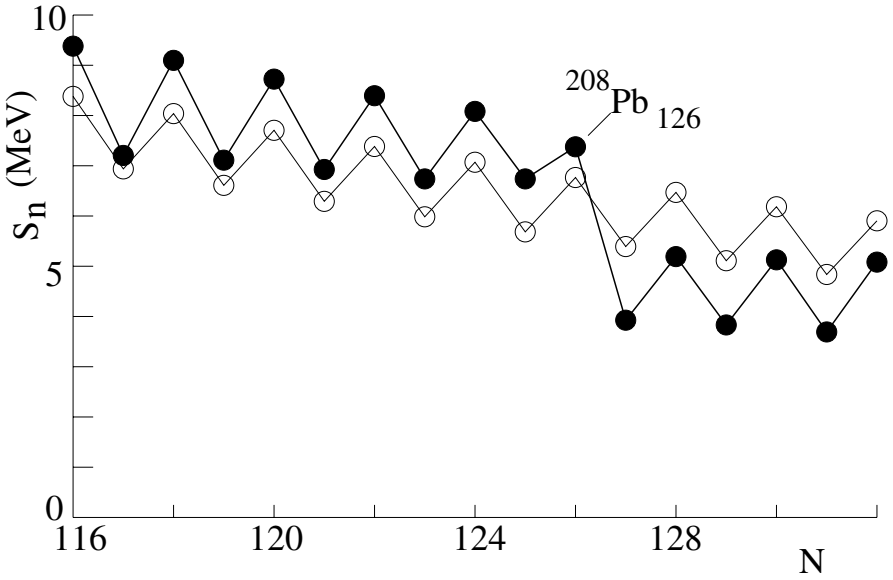

Fig. 2.7. The neutron separation energy in lead isotopes as a function of N. The filled dots show the measured values and the open dots show the predictions of the Bethe–Weizsäcker formula.

The discontinuity in the separation energies is due to the excess binding energy for magic nuclei as compared to that predicted by the semi-empirical Bethe–Weizsäcker mass formula. One can see this in Fig. 2.8 which plots the excess binding energy as a function of N and Z. Large positive values of B/A(experimental)-B/A(theory) are observed in the vicinity of the magic numbers for neutrons N as well as for protons Z. Figure 2.9 shows the difference as a function of N and Z in the vicinity of the magic numbers 28, 50, 82 and 126.

Just as the energy necessary to liberate a neutron is especially large at magic numbers, the difference in energy between the nuclear ground state and the first excited state is especially large for these nuclei. Table 2.1 gives this energy as a function of N (even) for Hg ($Z = 80$), Pb ($Z = 82$) and Po ($Z = 84$). Only even–even nuclei are considered since these all have similar nucleon structures with the ground state having $J^P = 0^+$ and a first excited state generally having $J^P = 2^+$. The table shows a strong peak at the doubly magic ^{208}Pb. As discussed in Sect. 1.3, the large energy difference between rotation

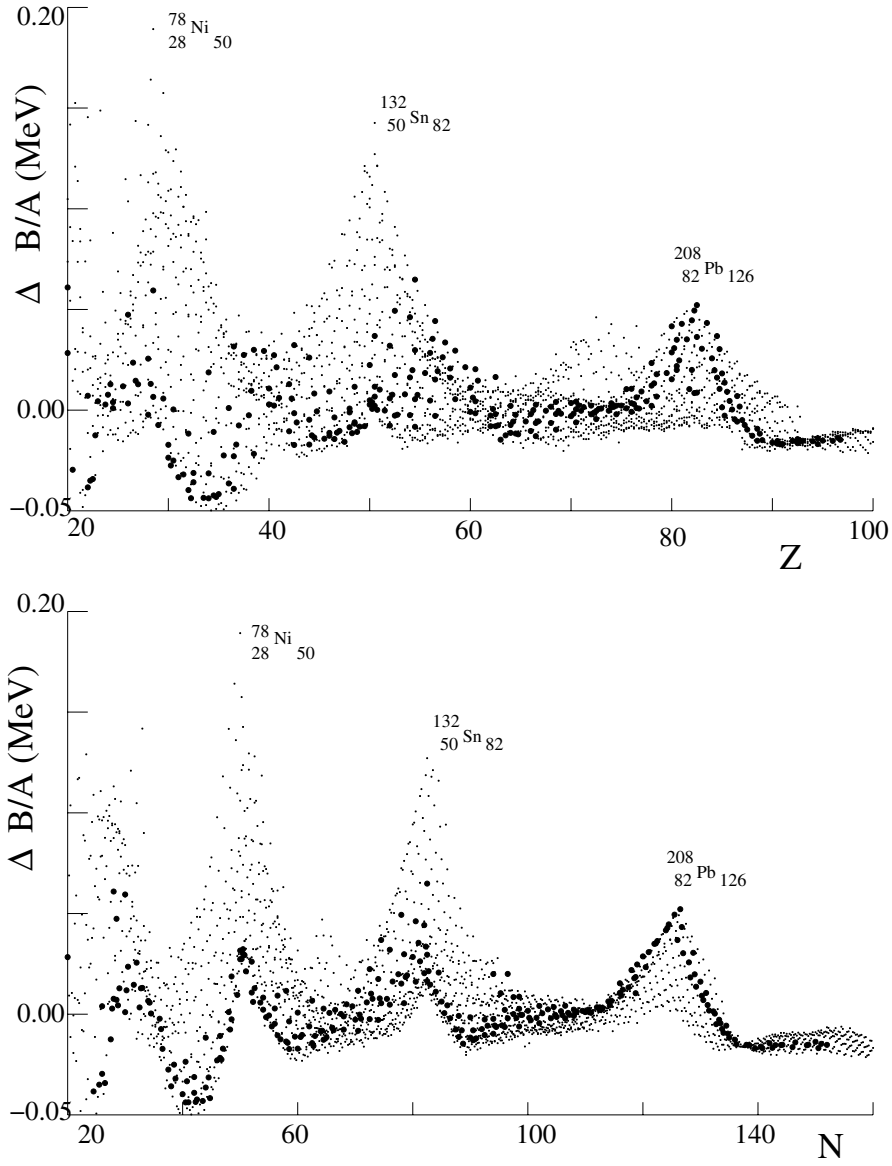

Fig. 2.8. Difference in MeV between the measured value of B/A and the value calculated with the empirical mass formula as a function of the number of protons Z (top) and of the number of neutrons N (bottom). The large dots are for β-stable nuclei. One can see maxima for the magic numbers $Z, N = 20$, 28, 50, 82, and 126. The largest excesses are for the doubly magic nuclides as indicated.

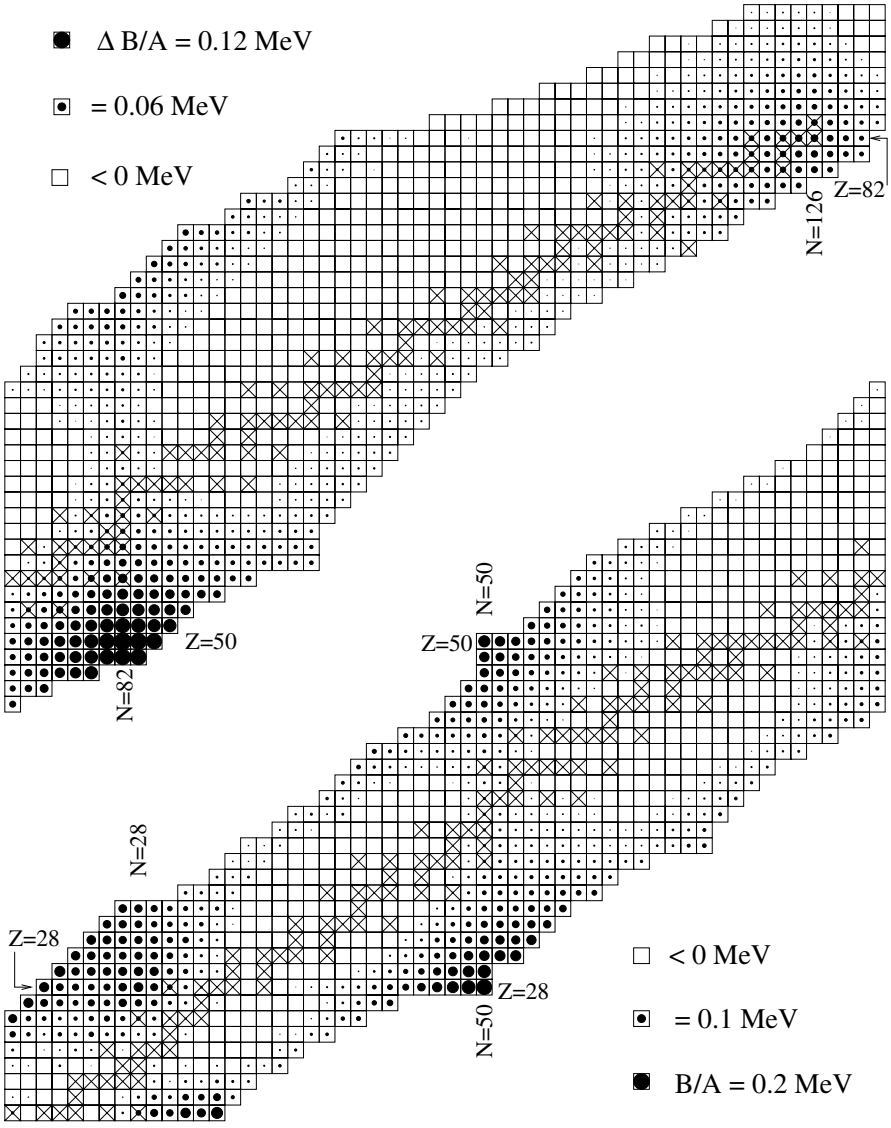

Fig. 2.9. Difference between the measured value of B/A and the value calculated with the mass formula as a function of N and Z. The size of the black dot increases with the difference. One can see the hills corresponding to the values of the magic numbers 28,50,82 and 126. Crosses mark β-stable nuclei.

states for ^{208}Pb is due to its sphericity. Sphericity is a general characteristic of magic nuclides, as illustrated in Fig. 1.8.

Table 2.1. The energy difference (keV) between the ground state (0^+) and the first excited state (2^+) for even–even isotopes of mercury ($Z = 80$), lead ($Z = 82$) and polonium ($Z = 84$). The largest energy difference is for the the double-magic ^{208}Pb. As discussed in Sect. 1.3, this large difference between rotational states is due to the sphericity of ^{208}Pb.

N→	112	114	116	118	120	122	124	126	128	130	132
Hg	423	428	426	412	370	440	436	1068			
Pb	260	171	304	1027	960	900	803	2614	800	808	837
Po	463	605	665	677	684	700	687	1181	727	610	540

2.4.1 The shell model and the spin-orbit interaction

It is possible to understand the nuclear shell structure within the framework of a modified mean field model. If we assume that the mean potential energy is harmonic, the energy levels are

$$E_n \;=\; (n + 3/2)\hbar\omega \qquad n \;=\; n_x + n_y + n_z = 0, 1, 2, 3 \ldots \;, \tag{2.38}$$

where $n_{x,y,z}$ are the quantum numbers for the three orthogonal directions and can take on positive semi-definite integers. If we fill up a harmonic well with nucleons, 2 can be placed in the one $n = 0$ orbital, i.e. the $(n_x, n_y, n_z) = (0, 0, 0)$. We can place 6 in the $n = 1$ level because there are 3 orbitals, $(1, 0, 0)$, $(0, 1, 0)$ and $(0, 0, 1)$. The number $N(n)$ are listed in the third row of Table 2.2.

We note that the harmonic potential, like the Coulomb potential, has the peculiarity that the energies depend only on the principal quantum number n and not on the angular momentum quantum number l. The angular momentum states, $|n, l, m\rangle$ can be constructed by taking linear combinations of the $|n_x, n_y, n_z\rangle$ states (Exercise 2.4). The allowed values of l for each n are shown in the second line of Table 2.2.

Table 2.2. The number N of nucleons per shell for a harmonic potential.

n	0	1	2	3	4	5	6
l	0	1	0,2	1,3	0,2,4	1,3,5	0,2,4,6
$N(n)$	2	6	12	20	30	42	56
$\sum N$	2	8	20	40	70	112	168

The magic numbers corresponding to all shells filled below the maximum n, as shown on the fourth line of Table 2.2, would then be 2, 8, 20, 40, 70, 112 and 168 in disagreement with observation (2.37). It might be expected that one could find another simple potential that would give the correct numbers. In general one would find that energies would depend on *two* quantum numbers: the angular momentum quantum number l and a second giving the number of nodes of the radial wavefunction. An example of such a *l-splitting* is shown in Fig. 2.10. Unfortunately, it turns out that there is no simple potential that gives the correct magic numbers.

The solution to this problem, found in 1949 by M. Göppert Mayer, and by D. Haxel J. Jensen and H. Suess, is to add a spin orbit interaction for each nucleon:

$$\hat{H} = V_{\mathrm{s-o}}(r)\hat{\boldsymbol{\ell}} \cdot \hat{\boldsymbol{s}}/\hbar^2 \ . \tag{2.39}$$

Without the spin-orbit term, the energy does not depend on whether the nucleon spin is aligned or anti-aligned with the orbital angular momentum. The spin orbit term breaks the degeneracy so that the energy now depends on three quantum numbers, the principal number n, the orbital angular momentum quantum number l and the total angular momentum quantum number $j = l \pm 1/2$. We note that the expectation value of $\hat{\boldsymbol{\ell}} \cdot \hat{\boldsymbol{s}}$ is (Exercise 2.5) given by

$$\begin{aligned} \frac{\hat{\boldsymbol{\ell}} \cdot \hat{\boldsymbol{s}}}{\hbar^2} &= \frac{j(j+1) - l(l+1) - s(s+1)}{2} \qquad s = 1/2 \ . \\ &= l/2 \qquad\quad \text{for } j = l + 1/2 \\ &= -(l+1)/2 \quad \text{for } j = l - 1/2 \ . \end{aligned} \tag{2.40}$$

For a given value of n, the energy levels are then changed by an amount proportional to this function of j and l. For $V_{\mathrm{s-o}} < 0$ the states with the spin aligned with the orbital angular momentum ($j = l + 1/2$) have their energies lowered while the states with the spin anti-aligned ($j = l - 1/2$) have their energies raised.

The orbitals with this interaction included (with an appropriately chosen $V_{\mathrm{s-o}}$) are shown in Fig. 2.10. The predicted magic numbers correspond to orbitals with a large gap separating them from the next highest orbital. For the lowest levels, the spin-orbit splitting (2.40) is sufficiently small that the original magic numbers, 2, 8, and 20, are retained. For the higher levels, the splitting becomes important and the gaps now appear at the numbers 28, 50, 82 and 126. This agrees with the observed quantum numbers (2.37). We note that this model predicts that the number 184 should be magic.

Besides predicting the correct magic numbers, the shell model also correctly predicts the spins and parities of many nuclear states. The ground states of even–even nuclei are expected to be 0^+ because all nucleons are paired with a partner of opposite angular momentum. The ground states of

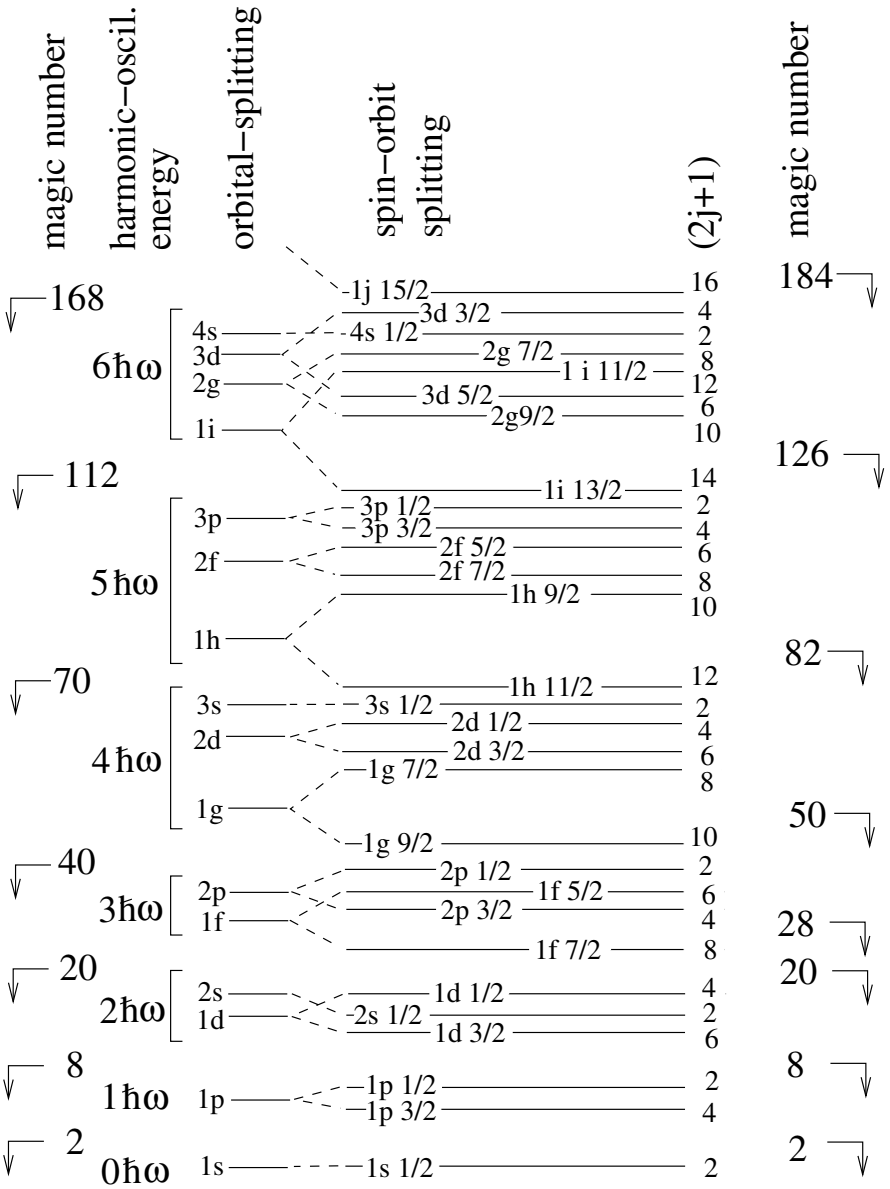

Fig. 2.10. Nucleon orbitals in a model with a spin-orbit interaction. The two left-most columns show the magic numbers and energies for a pure harmonic potential. The splitting of different values of the orbital angular momentum l can be arranged by modifying the central potential. Finally, the spin-orbit coupling splits the levels so that they depend on the relative orientation of the spin and orbital angular momentum. The number of nucleons per level $(2j + 1)$ and the resulting magic numbers are shown on the right.

odd–even nuclei should then take the quantum numbers of the one unpaired nucleon. For example, ${}^{17}_{9}\mathrm{F}_8$ and ${}^{17}_{8}\mathrm{O}_9$ have one unpaired nucleon outside a doubly magic ${}^{16}_{8}\mathrm{O}_8$ core. Figure 2.10 tells us that the unpaired nucleon is in a $l = 2$, $j = 5/2$. The spin parity of the nucleus is predicted to by $5/2^+$ since the parity of the orbital is -1^l. This agrees with observation. The first excited states of ${}^{17}_{9}\mathrm{F}_8$ and ${}^{17}_{8}\mathrm{O}_9$, corresponding to raising the unpaired nucleon to the next higher orbital, are predicted to be $1/2^+$, once again in agreement with observation.

On the other hand, ${}^{15}_{8}\mathrm{N}_7$ and ${}^{15}_{8}\mathrm{O}_7$ have one "hole" in their ${}^{16}\mathrm{O}$ core. The ground state quantum numbers should then be the quantum numbers of the hole which are $l = 1$ and $j = 1/2$ according to Fig. 2.10. The quantum numbers of the ground state are then predicted to be $1/2^-$, in agreement with observation.

The shell model also makes predictions for nuclear magnetic moments . As for the total angular momentum, the magnetic moments results from a combination of the spin and orbital angular momentum. However, in this case, the weighting is different because the gyromagnetic ratio of the spin differs from that of the orbital angular momentum. This problem is explored in Exercise 2.7.

Shell model calculations are important in many other aspects of nuclear physics, for example in the calculation of β-decay rates. The calculations are quite complicated and are beyond the scope of this book. Interested readers are referred to the advanced textbooks.

2.4.2 Some consequences of nuclear shell structure

Nuclear shell structure is reflected in many nuclear properties and in the relative natural abundances of nuclei. This is especially true for doubly magic nuclei like ${}^{4}\mathrm{He}_2$, ${}^{16}\mathrm{O}_8$ and ${}^{40}\mathrm{Ca}_{20}$ all of which have especially large binding energies. The natural abundances of ${}^{40}\mathrm{Ca}$ is 97% while that of ${}^{44}\mathrm{Ca}_{24}$ is only 2% in spite of the fact that the semi-empirical mass formula predicts a greater binding energy for ${}^{44}\mathrm{Ca}$. The doubly magic ${}^{100}\mathrm{Sn}_{50}$ is far from the stability line (${}^{100}\mathrm{Ru}_{56}$) but has an exceptionally long half-life of 0.94 s. The same can be said for , ${}^{48}\mathrm{Ni}_{20}$, the mirror of ${}^{48}\mathrm{Ca}_{28}$ which is also doubly magic. ${}^{56}\mathrm{Ni}_{28}$ is the final nucleus produced in stars before decaying to ${}^{56}\mathrm{Co}$ and then ${}^{56}\mathrm{Fe}$ (Chap. 8). Finally, ${}^{208}_{82}\mathrm{Pb}_{126}$ is the only heavy double-magic. It, along with its neighbors ${}^{206}\mathrm{Pb}$ and ${}^{207}\mathrm{Pb}$, are the final states of the three natural radioactive chains shown in Fig. 5.2.

Nuclei with only one closed shell are called "semi-magic":

- isotopes of nickel, $Z = 28$;
- isotopes of tin, $Z = 50$;
- isotopes of lead, $Z = 82$;
- isotones $N = 28$ (${}^{50}\mathrm{Ti}$, ${}^{51}\mathrm{V}$, ${}^{52}\mathrm{Cr}$,${}^{54}\mathrm{Fe}$, etc.)
- isotones $N = 50$ (${}^{86}\mathrm{Kr}$, ${}^{87}\mathrm{Rb}$, ${}^{88}\mathrm{Sr}$, ${}^{89}\mathrm{Y}$, ${}^{90}\mathrm{Zr}$, etc.)

- isotones $N = 82$ (^{136}Xe, ^{138}Ba, ^{139}La, ^{140}Ce, ^{141}Pr, etc.)

These nuclei have

- a binding energy greater than that predicted by the semi-empirical mass formula,
- a large number of stable isotopes or isotones,
- a large natural abundances,
- a large energy separation from the first excited state,
- a small neutron capture cross-section (magic-N only).

The exceptionally large binding energy of doubly magic ^{4}He makes α decay the preferred mode of A non-conserving decays. Nuclei with $209 < A < 240$ all cascade via a series of β and α decays to stable isotopes of lead and thallium. Even the light nuclei ^{5}He, ^{5}Li and ^{8}Be decay by α emission with lifetimes of order 10^{-16} s.

While ^{5}He rapidly α decays, ^{6}He has a relatively long lifetime of 806 ms. This nucleus can be considered to be a three-body state consisting of 2 neutrons and an α particle. This system has the peculiarity that while being stable, none of the two-body subsystems (n-n or n-α) are stable. Such systems are called "Borromean" after three brothers from the Borromeo family of Milan. The three brothers were very close and their coat-of-arms showed three rings configured so that breaking any one ring would separate the other two.

Shell structure is a necessary ingredient in the explanation of nuclear deformation. We note that the Bethe–Weizsäcker mass formula predicts that nuclei should be spherical, since any deformation at constant volume increases the surface term. This can be quantified by a "deformation potential energy" as illustrated in Fig. 2.11. In the liquid-drop model a local minimum is found at vanishing deformation corresponding to spherical nuclei. If the nucleus is unstable to spontaneous fission, the absolute minimum is at large deformation corresponding to two separated fission fragments (Chap. 6).

Since the liquid-drop model predicts spherical nuclei, observed deformation must be due to nuclear shell structure. Deformations are then linked to how nucleons fill available orbitals. For instance, even–even nuclei have paired nucleons. As illustrated in Fig. 2.12, if the nucleons tend to populate the high-m orbitals of the outer shell of angular momentum l, then the nucleus will be oblate. If they tend to populate low-m orbitals, the nucleus will be prolate. Which of these cases occurs depends on the details of the complicated nuclear Hamiltonian. The most deformed nuclei are prolate.

Because of these quantum effects, the deformation energy in Fig. 2.11 will have a local minimum at non-vanishing deformation for non-magic nuclei. It is also possible that a local minimum occurs for super-deformed configurations. These metastable configurations are seen in rotation band spectra, e.g. Fig. 1.9.

We note that the shell model predicts and "island of stability" of superheavy nuclei near the magic number $(A, N, Z) = (298, 184, 114)$ and (310,

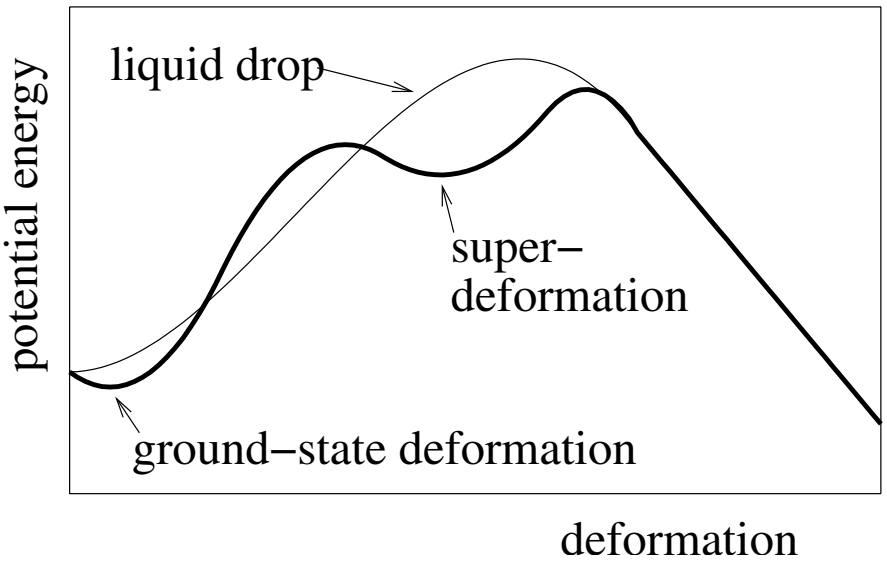

Fig. 2.11. Nuclear energies as a function of deformation. The liquid-drop model predicts that the energy has a local minimum for vanishing deformation because this minimizes the surface energy term. (As discussed in Chap. 6, in high-Z nuclei the energy eventually decreases for large deformations because of Coulomb repulsion, leading to spontaneous fission of the nucleus.) As explained in the text, the shell structure leads to a deformation of the ground state for nuclei with unfilled shells. Super-deformed local minima may also exist.

184, 126). The lifetimes are estimated to be as high as 10^6 yr making them of more than purely scientific interest. As discussed in Sect. 2.8, attempts to approach this island are actively pursued.

Finally, we mention that an active area or research concerns the study of magic numbers for neutron-rich nuclei far from the bottom of the stability valley. It is suspected that for such nuclides the shell structure is modified. This effect is important for the calculation of nucleosynthesis in the *r-process* (Sect. 8.3).

2.5 β-instability

As already emphasized, nuclei with a non-optimal neutron-to-proton ratio can decay in A-conserving β-decays. As illustrated in Fig. 2.6, nuclei with an excess of neutrons will β^- decay:

$$(A, Z) \rightarrow (A, Z+1)\, \mathrm{e}^- \bar{\nu}_\mathrm{e} \tag{2.41}$$

which is the nuclear equivalent of the more fundamental particle reaction

$$\mathrm{n} \rightarrow \mathrm{p} + \mathrm{e}^- + \bar{\nu}_\mathrm{e}\ . \tag{2.42}$$

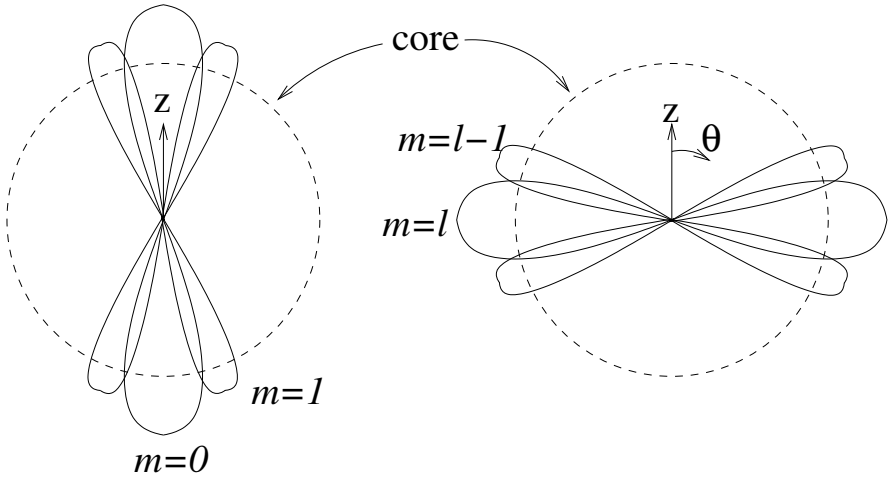

Fig. 2.12. The distribution of polar angle θ for high-l orbitals with respect to the symmetry (z) axis. In 0^+ nuclei, nucleons pair up in orbitals of opposite angular momentum. In partially-filled shells, only some of the m orbitals will be filled. If the pairs populate preferentially low $|m|$ orbitals, as on the left, the nucleus will take a deformed prolate shape. If the pairs populate preferentially high $|m|$ orbitals, as on the right, the nucleus will take an oblate shape. The spherical core of filled shells is also shown.

Nuclei with an excess of protons will either β^+ decay

$$(A, Z) \rightarrow (A, Z-1)\, \mathrm{e}^+ \bar{\nu}_\mathrm{e} \tag{2.43}$$

or, if surrounded by atomic electrons, decay by electron capture

$$\mathrm{e}^- \,(\mathrm{A}, \mathrm{Z}) \rightarrow (\mathrm{A}, \mathrm{Z}-1)\, \bar{\nu}_\mathrm{e} \quad . \tag{2.44}$$

These two reactions are the nuclear equivalents of the particle reactions

$$\mathrm{e}^- \,\mathrm{p} \rightarrow \mathrm{n}\, \nu_\mathrm{e} \qquad \mathrm{p} \rightarrow \mathrm{n}\, \mathrm{e}^+ \nu_\mathrm{e} \,. \tag{2.45}$$

In order to conserve energy-momentum, proton β^+-decay is only possible in nuclei.

The energy release in β^--decay is given by

$$\begin{aligned} Q_{\beta^-} &= m(A,Z) - m(A,Z+1) - m_\mathrm{e} \\ &= (B(A,Z+1) - B(A,Z)) + (m_\mathrm{n} - m_\mathrm{p} - m_\mathrm{e}) \end{aligned} \tag{2.46}$$

while that in β^+-decay is

$$\begin{aligned} Q_{\beta^+} &= m(A,Z) - m(A,Z-1) - m_\mathrm{e} \\ &= (B(A,Z-1) - B(A,Z)) - (m_\mathrm{n} - m_\mathrm{p} - m_\mathrm{e}) \,. \end{aligned} \tag{2.47}$$

The energy release in electron capture is larger than that in β^+-decay

$$Q_{\rm ec} \;=\; Q_{\beta^+} + 2m_{\rm e} \tag{2.48}$$

so electron capture is the only decay mode available for neighboring nuclei separated by less than $m_{\rm e}$ in mass.

The energy released in β-decay can be estimated from the semi-empirical mass formula. For moderately heavy nuclei we can ignore the Coulomb term and the estimate is

$$Q_\beta \;\sim\; \frac{8a_{\rm a}}{A}\,|Z - A/2| \;\sim\; \frac{100\,{\rm MeV}}{A}\;. \tag{2.49}$$

As with all reactions in nuclear physics, the Q values are in the MeV range.

β-decays and electron captures are governed by the weak interaction. The fundamental physics involved will be discussed in more detail in Chap. 4. One of the results will be that for $Q_\beta \gg m_{\rm e}$, the decay rate is proportional to the fifth power of Q_β

$$\lambda_\beta \;\propto\; G_{\rm F}^2\,Q_\beta^5 \;\sim\; 10^{-4}{\rm s}^{-1}\left(\frac{Q_\beta}{1\,{\rm MeV}}\right)^5 \qquad Q_\beta \gg m_{\rm e}c^2 \tag{2.50}$$

where the Fermi constant $G_{\rm F}$, given by $G_{\rm F}/(\hbar c)^3 = 1.166\,10^{-5}$ GeV^{-2}, is the effective coupling constant for low-energy weak interactions. The constant of proportionality depends in the details of the initial and final state nuclear wavefunctions. In the most favorable situations, the constant is of order unity.

Figure 2.13 shows the lifetimes of β emitters as a function of Q_β. The line shows the maximum allowed rate, which, for $Q_\beta \gg m_{\rm e}c^2$, is $\sim (G_{\rm F}^2 Q^5)^{-1}$. For $Q_\beta < 1\,{\rm MeV}$, lifetimes of β^+ emitters are shorter that those of β^- emitters because of the contribution of electron capture.

Electron captures are also governed by the weak interactions and, as such, capture rates are proportional to $G_{\rm F}^2$. We will see in Chap. 4 that the decay rate is roughly

$$\lambda_{\rm ec} \;\propto\; (\alpha Z m_{\rm e}c^2)^3 G_{\rm F}^2\,Q_{\rm ec}^2\;, \tag{2.51}$$

where $\alpha \sim 1/137$ is the fine structure constant. The strong Z dependence comes from the fact that the decay rate is proportional to the probability that an electron is near the nucleus, i.e. the square of the wavefunction at the origin for the inner electrons. This probability is inversely proportional to the third power of the effective Bohr radius of the inner shell atomic electrons. This gives the factor in parentheses in the decay rate.

For nuclei that can decay by both electron capture and β^+-decay, the ratio between the two rates is given by

$$\frac{\lambda_{\rm ec}}{\lambda_{\beta^+}} \;\sim\; (Z\alpha)^3\,\frac{Q_{\rm ec}^2(m_{\rm e}c^2)^3}{(Q_{\rm ec} - 2m_{\rm e}c^2)^5} \qquad Q_{\rm ec} > 2m_{\rm e}c^2\;. \tag{2.52}$$

We see that electron capture is favored for high Z and low $Q_{\rm ec}$, while β^+ is favored for low Z and high $Q_{\rm ec}$.

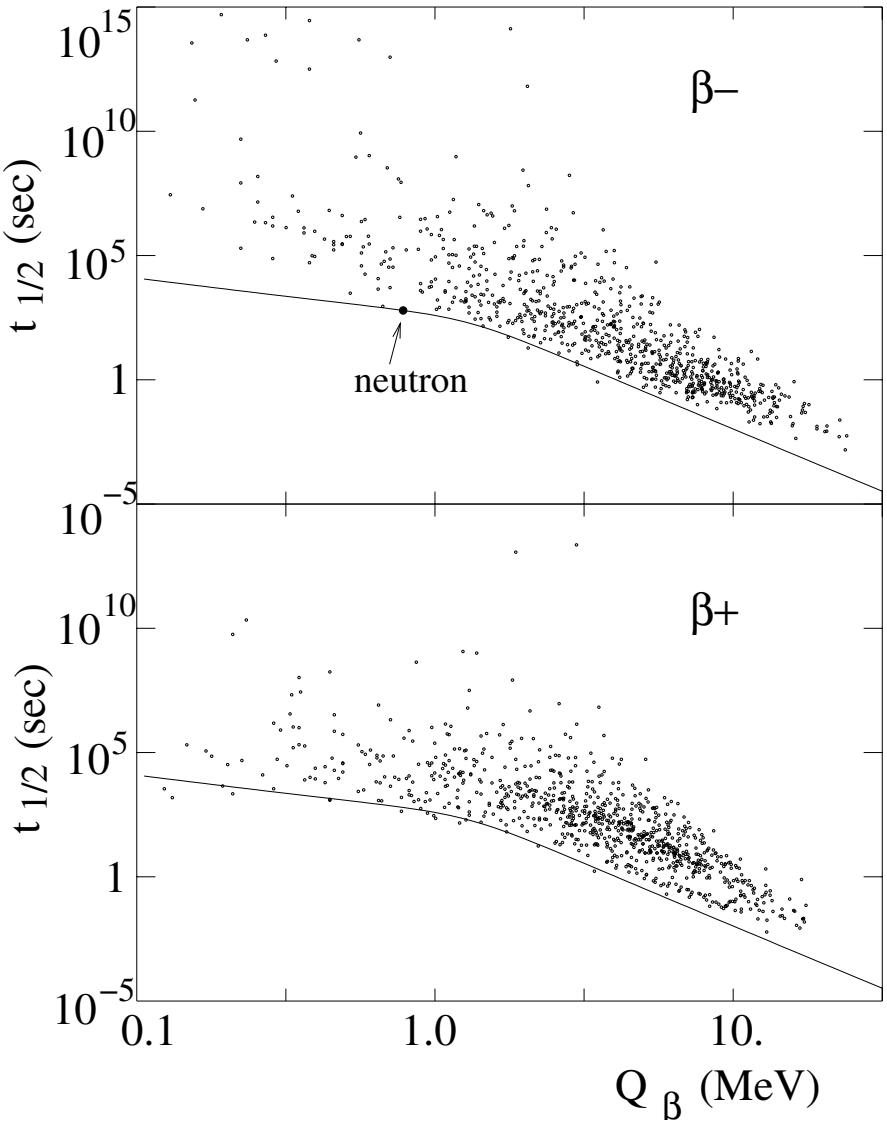

Fig. 2.13. The half-lives of β^- (top) and β^+ (bottom) emitters as a function of Q_β. The line corresponds to the maximum allowable β decay rate which, for $Q_\beta \gg m_e c^2$ is given by $t_{1/2}^{-1} \sim G_F^2 Q_\beta^2$. The complete Q_β dependence will be calculated in Chap. 4. For $Q_\beta < 1\,\mathrm{MeV}$, the lifetimes of β^+ emitters are shorter than those for β^- emitters because of the contribution of electron-capture.

As seen in Fig. 2.13, β-decay lifetimes range from seconds to years. Examples are $\sim 10^{-5}$ s for ^{7}He and $\sim 10^{24}$ s for ^{50}V. The reasons for this large range will be discussed in Chap. 4.

2.6 α-instability

Because nuclear binding energies are maximized for $A \sim 60$, heavy nuclei that are β-stable (or unstable) can generally split into more strongly bound lighter nuclei. Such decays are called "spontaneous fission." The most common form of fission is α-decay:

$$(A, Z) \;\rightarrow\; (A-4, Z-2) \;+\; {}^{4}\mathrm{He} \quad , \tag{2.53}$$

for example

- $^{232}\mathrm{Th}_{90} \rightarrow {}^{228}\mathrm{Ra}_{88}\ \alpha\ + 4.08\mathrm{MeV} \quad ; \quad \mathrm{t}_{1/2}\ = 1.4\ 10^{10}\,\mathrm{yr}$
- $^{224}\mathrm{Th}_{90} \rightarrow {}^{220}\mathrm{Ra}_{88}\ \alpha\ + 7.31\mathrm{MeV} \quad ; \quad \mathrm{t}_{1/2}\ = 1.05\,\mathrm{s}$
- $^{142}\mathrm{Ce}_{58} \rightarrow {}^{138}\mathrm{Ba}_{56}\ \alpha\ + 1.45\mathrm{MeV} \quad ; \quad \mathrm{t}_{1/2}\ \sim 5.10^{15}\,\mathrm{yr}$
- $^{212}\mathrm{Po}_{84} \rightarrow {}^{208}\mathrm{Pb}_{82}\ \alpha\ + 8.95\mathrm{MeV} \quad ; \quad \mathrm{t}_{1/2}\ = 3.10^{-7}\mathrm{s}$

Figure 2.14 shows the energy release, Q_α in α-decay for β-stable nuclei. We see that most nuclei with $A > 140$ are potential α-emitters. However, naturally occurring nuclides with α-half-lives short enough to be observed have either $A > 208$ or $A \sim 145$ with ^{142}Ce being lightest.

The most remarkable characteristic of α-decay is that the decay rate is an exponentially increasing function of Q_α. This important fact is spectacularly demonstrated by comparing the lifetimes of various uranium isotopes:

- $^{238}\mathrm{U} \rightarrow {}^{234}\mathrm{Th}\ \alpha + 4.19\,\mathrm{MeV} \quad ; \quad \mathrm{t}_{1/2} = 1.4 \times 10^{17}\,\mathrm{s}$
- $^{236}\mathrm{U} \rightarrow {}^{232}\mathrm{Th}\ \alpha + 4.45\,\mathrm{MeV} \quad ; \quad \mathrm{t}_{1/2} = 7.3 \times 10^{14}\,\mathrm{s}$
- $^{234}\mathrm{U} \rightarrow {}^{230}\mathrm{Th}\ \alpha + 4.70\,\mathrm{MeV} \quad ; \quad \mathrm{t}_{1/2} = 7.8 \times 10^{12}\,\mathrm{s}$
- $^{232}\mathrm{U} \rightarrow {}^{228}\mathrm{Th}\ \alpha + 5.21\,\mathrm{MeV} \quad ; \quad \mathrm{t}_{1/2} = 2.3 \times 10^{9}\,\mathrm{s}$
- $^{230}\mathrm{U} \rightarrow {}^{226}\mathrm{Th}\ \alpha + 5.60\,\mathrm{MeV} \quad ; \quad \mathrm{t}_{1/2} = 1.8 \times 10^{6}\,\mathrm{s}$
- $^{228}\mathrm{U} \rightarrow {}^{224}\mathrm{Th}\ \alpha + 6.59\,\mathrm{MeV} \quad ; \quad \mathrm{t}_{1/2} = 5.6 \times 10^{2}\,\mathrm{s}$

The lifetimes of other α-emitters are shown in Fig. 2.61.

This strong Q_α dependence can be understood within the framework of a model introduced by Gamow in 1928. In this model, a nucleus is considered to contain α-particles bound in the nuclear potential. If the electrostatic interaction between an α and the rest of the nucleus is "turned off," the α's potential is that of Fig. 2.16a. As usual, the potential has a range R and a depth V_0. Its binding energy is called E_α. In this situation, the nucleus is completely stable against α-decay.

If we now "turn on" the electrostatic potential between the α and the rest of the nucleus, E_α increases because of the repulsion. For highly charged heavy nuclei, the increase in E_α can be sufficient to make $E_\alpha > 0$, a situation shown in Fig. 2.16b. Such a nucleus, classically stable, can decay quantum

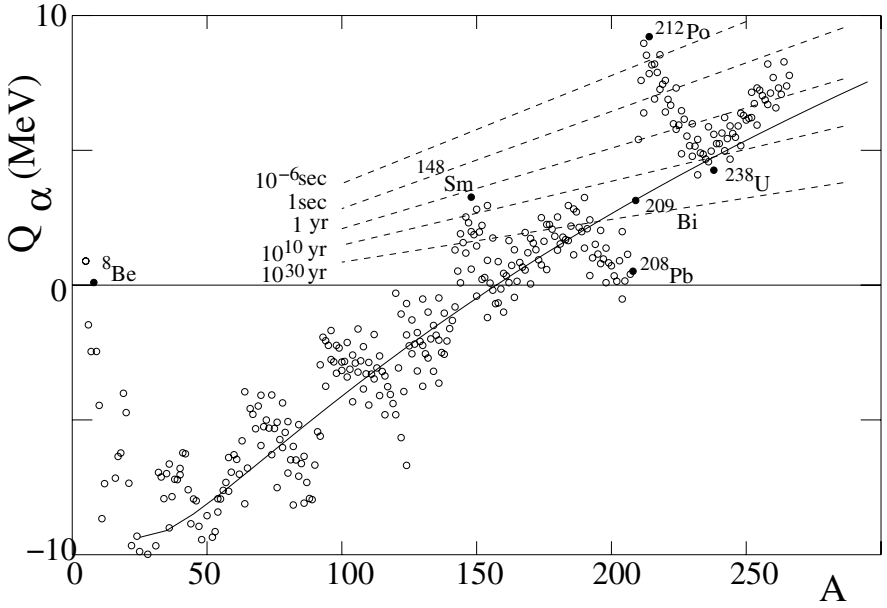

Fig. 2.14. Q_α vs. A for β-stable nuclei. The solid line shows the prediction of the semi-empirical mass formula. Because of the shell structure, nuclei just heavier than the doubly magic ^{208}Pb have large values of Q_α while nuclei just lighter have small values of Q_α. The dashed lines show half-lives calculated according to the Gamow formula (2.61). Most nuclei with $A > 140$ are potential α-emitters, though, because of the strong dependence of the lifetime on Q_α, the only nuclei with lifetimes short enough to be observed are those with $A > 209$ or $A \sim 148$, as well as the light nuclei ^{8}Be, ^{5}Li, and ^{5}He.

mechanically by the tunnel effect. The tunneling probability could be trivially calculated if the potential barrier where a constant energy V of width Δ:

$$P \propto \text{cte}\; e^{-2K\Delta}\;, \qquad K = \sqrt{\frac{2m(V-E_\alpha)}{\hbar^2}} \quad . \tag{2.54}$$

To calculate the tunneling probability for the potential of Fig. 2.16b, it is sufficient to replace the potential with a series of piece-wise constant potentials between $r = R$ and $r = b$ and then to sum:

$$P \;\propto\; \mathrm{e}^{-2\gamma} \qquad \gamma \;=\; \int_R^b \sqrt{\frac{2(V(r)-E_\alpha)mc^2}{\hbar^2c^2}}\mathrm{d}r \tag{2.55}$$

where $V(r)$ is the potential in Fig. 2.16b. The rigorous justification of this formula comes from the WKB approximation studied in Exercise 2.9.

The integral in (2.55) can be simplified by defining the dimensionless variable

$$u \;=\; \frac{E}{V(r)} \;=\; r\,\frac{E}{2(Z-2)\alpha\hbar c}\;. \tag{2.56}$$

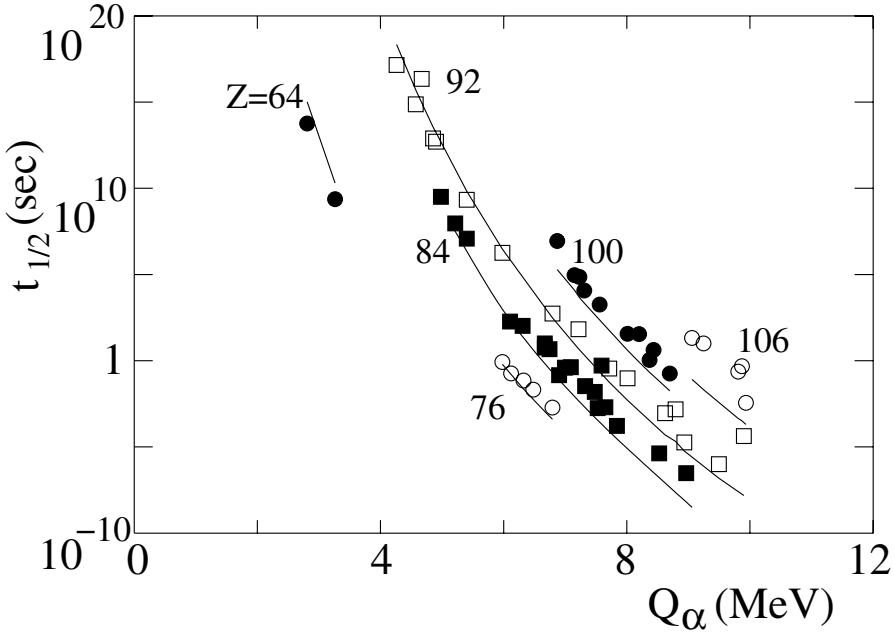

Fig. 2.15. The half-lives vs. Q_α for selected nuclei. The half-lives vary by 23 orders of magnitude while Q_α varies by only a factor of two. The lines shown the prediction of the Gamow formula (2.61).

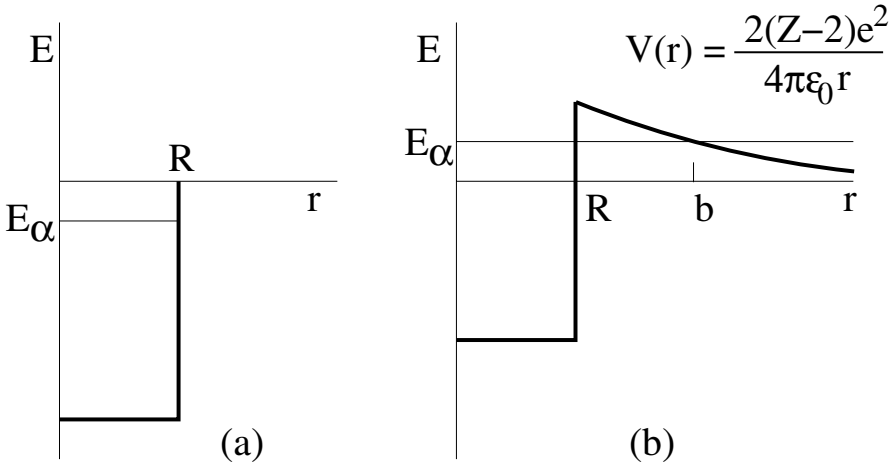

Fig. 2.16. Gamow's model of α-decay in which the nucleus contains a α-particle moving in a mean potential. If the electromagnetic interactions are "turned off", the α-particle is in the state shown on the left. When the electromagnetic interaction is turned on, the energy of the α-particle is raised to a position where it can tunnel out of the nucleus.

We then have

$$\gamma \;=\; \frac{2(Z-2)e^2}{4\pi\epsilon_0\hbar}\sqrt{\frac{2m_\alpha}{E}}\int_{u_{\min}}^{1}\sqrt{u^{-1}-1}\,\mathrm{d}u\;. \tag{2.57}$$

For large Z, (2.56) suggests that it is a reasonably good approximation to take $u_{\min}=0$ in which case the integral is $\pi/2$. This gives

$$\gamma = 2\pi(Z-2)\alpha\,\frac{c}{v} \tag{2.58}$$

where $v=\sqrt{2E/m_\alpha}$ is the velocity of the α-particle after leaving the nucleus. For ^{238}U we have $2\gamma\sim 172$ while for ^{228}U we have $2\gamma\sim 136$. We see how the small difference in energy leads to about 16 orders of magnitude difference in tunneling probability and, therefore, in lifetime.

To get a better estimate of the lifetime, we have to take into account the fact that $u_{\min}>0$. This increases the tunneling probability since the barrier width is decreased. It is simple to show (Exercise 2.8) that to good approximation

$$\gamma = \frac{2Z}{\sqrt{(E_\alpha(MeV))}} - \frac{3}{2}\sqrt{ZR(fm)} \quad . \tag{2.59}$$

The dependence of the lifetime of the nuclear radius provided one of the first methods to estimate nuclear radii.

The lifetime can be calculated by supposing that inside the nucleus the α bounces back and forth inside the potential. Each time it hits the barrier it has a probability P to penetrate. The mean lifetime is then just T/P where $T\sim R/v'$ is the oscillation frequency for the α of velocity $v'=\sqrt{2m_\alpha(E_\alpha+V_0)}$. This induces an additional Q_α dependence of the lifetime which is very weak compared to the exponential dependence on Q_α due to the tunneling probability. If we take the logarithm of the lifetime, we can safely ignore this dependence on Q_α, so, to good approximation, we have

$$\ln\tau(Q_\alpha,Z,A) \;=\; 2\gamma \,+\, \text{const}\;, \tag{2.60}$$

with γ given by (2.15). Numerically, one finds

$$\log(t_{1/2}/1\,\mathrm{s}) \;\sim\; 2\gamma/\ln 10 \,+\, 25\;, \tag{2.61}$$

which is the formula used for the lifetime contours in Figs. 2.14 and 2.15.

One consequence of the strong rate dependence on Q_α is the fact that α-decays are preferentially to the ground state of the daughter nucleus, since decays to excited states necessarily have smaller values of Q_α. This is illustrated in Fig. 2.17 in the case of the decay $^{228}\mathrm{U}\to\alpha\,^{228}\mathrm{Th}$. In β-decays, the Q_β dependence is weaker and many β-decays lead to excited states.

We note that the tunneling theory can also be applied to spontaneous fission decays where the nucleus splits into two nuclei of comparable mass and charge. In this case, the barrier is that of the deformation energy shown in Fig. 2.11. Note also that the decay

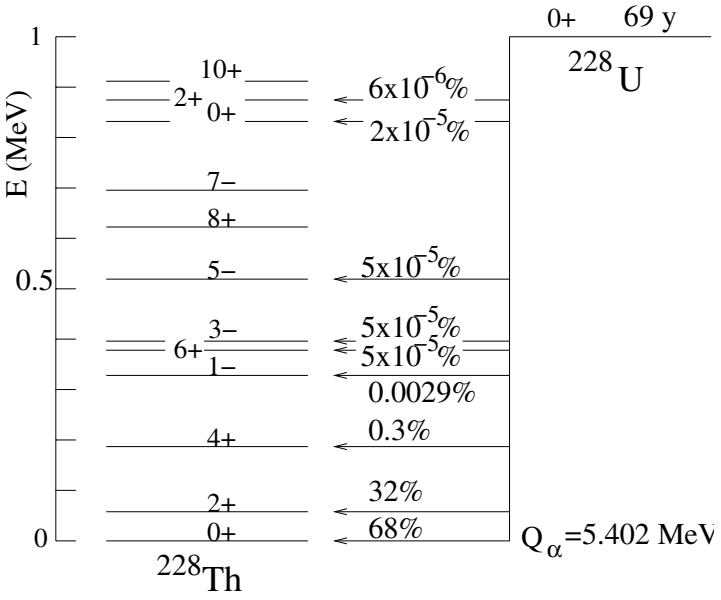

Fig. 2.17. The decay $^{228}\mathrm{U} \rightarrow \alpha\, ^{228}\mathrm{Th}$ showing the branching fractions to the various excited states of ^{228}Th. Because of the strong rate dependence on Q_α, the ground state his highly favored. There is also a slight favoring of spin-parities that are similar to that of the parent nucleus.

$$^{212}_{86}\mathrm{Rn} \rightarrow {}^{198}_{80}\mathrm{Hg}\, {}^{14}_{6}\mathrm{C} \tag{2.62}$$

has also been observed, providing an example intermediate between α decay and spontaneous fission.

2.7 Nucleon emission

An extreme example of nuclear fission is the emission of single nucleons. This is energetically possible if the condition (2.16) is met. This is the case for the ground states of all nuclides outside the proton and neutron drip-lines shown in Fig. 2.1. Because there is no Coulomb barrier for neutron emission and a much smaller barrier for proton emission than for α emission, nuclei that can decay by nucleon emission generally have lifetimes shorter than $\sim 10^{-20}$s.

While few nuclides have been observed whose ground states decay by nucleon emission, states that are sufficiently excited can decay in this way. This is especially true for nuclides just inside the drip-lines. An example is the proton rich nuclide ^{43}V whose proton separation energy is only 0.194 MeV. All excited states above this energy decay by proton emission. The observation of these decay is illustrated in Fig. 2.18. Another example if that of the neutron-rich nuclide ^{87}Br (Fig. 6.13). We will see that such nuclei have an important role in the operation of nuclear reactors.

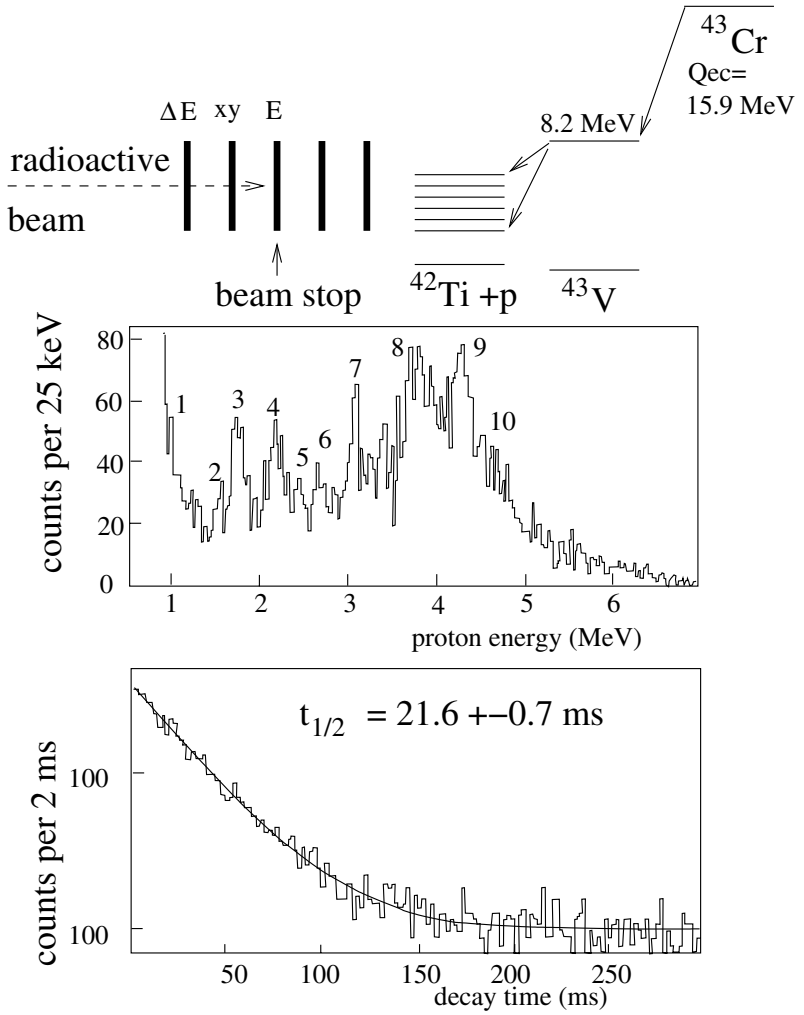

Fig. 2.18. The decay of the proton rich nuclide ^{43}Cr. Radioactive nuclei are produced in the fragmentation of 74.5 MeV/nucleon ^{58}Ni nuclei incident on a nickel target at GANIL [27]. After momentum selection, ions are implanted in a silicon diode (upper right). The (A, Z) of each implanted nucleus is determined from energy loss and position measurements as in Fig. 5.10. The implanted ^{43}Cr β-decays with via the scheme shown in the upper right, essentially to the 8.2 MeV excited state of ^{43}V. This state then decays by proton emission to ^{42}Ti. The proton deposits all its energy in the silicon diode containing the decaying ^{43}Cr and the spectrum of protons shows the position of excited states of ^{42}Ti. The bottom panel gives the distribution of time between the ion implantation and decay, indicating $t_{1/2}(^{43}\mathrm{Cr}) = 21.6 \pm 0.7$ ms.

Highly excited states that can emit neutrons appear is resonances in the cross-section of *low-energy* neutrons. Examples are shown in Fig. 3.26 for states of ^{236}U and ^{239}U that decay by neutron emission to ^{235}U and ^{238}U. These states are also important in the operation of nuclear reactors.

2.8 The production of super-heavy elements

One of the most well-known results of research in nuclear physics has been the production of "trans-uranium" elements that were not previously present on Earth. The first trans-uranium elements, neptunium and plutonium, were produced by neutron capture

$$\mathrm{n}\,^{238}\mathrm{U} \;\rightarrow\; ^{239}\mathrm{U}\,\gamma\,, \tag{2.63}$$

followed by the β-decays

$$^{239}\mathrm{U} \;\rightarrow\; ^{239}\mathrm{Np}\,\mathrm{e}^-\,\bar{\nu}_\mathrm{e} \qquad \mathrm{t}_{1/2} \;=\; 23.45\,\mathrm{m} \tag{2.64}$$

$$^{239}\mathrm{Np} \;\rightarrow\; ^{239}\mathrm{Pu}\,\mathrm{e}^-\,\bar{\nu}_\mathrm{e} \qquad \mathrm{t}_{1/2} \;=\; 2.3565\,\mathrm{day}\,. \tag{2.65}$$

The half-life of ^{239}Pu is sufficiently long, 2.4×10^4 yr, that it can be studied as a chemical element.

Further neutron captures on ^{239}Pu produce heavier elements. This is the source of trans-uranium radioactive wastes in nuclear reactors. As shown in Fig. 6.12, this process cannot produce nuclei heavier than $^{258}_{100}$Fm which decays sufficiently rapidly ($t_{1/2} = 0.3\,\mathrm{ms}$) that it does not have time to absorb a neutron.

Elements with $Z > 100$ can only be produced in heavy-ion collisions. Most have been produced by bombardment of a heavy element with a medium-A nucleus. Figure 2.19 shows how ^{260}Db (element 104) was positively identified via the reaction

$$^{15}\mathrm{N}\,^{249}\mathrm{Cf} \;\rightarrow\; ^{260}\mathrm{Db} \;+\; 4\mathrm{n}\,. \tag{2.66}$$

Neutrons are generally present in the final state since the initially produced compound nucleus, in this case ^{264}Db, generally emits (evaporates) neutrons until reaching a bound nucleus. Such reactions are called *fusion-evaporation* reactions.

The heaviest element produced so far is the unnamed element 116, produced as in Fig. 2.20 via the reaction [29]

$$^{48}_{20}\mathrm{Ca}\,^{248}_{96}\mathrm{Cm} \;\rightarrow\; ^{296}116\,. \tag{2.67}$$

A beam of ^{48}Ca is used because its large neutron excess facilitates the production of neutron-rich heavy nuclei.[3] As shown in the figure, a beam of ^{48}Ca

[3] Planned radioactive beams (Fig. 5.5) using neutron-rich fission products will increase the number of possible reactions, though at lower beam intensity.

ions of kinetic energy 240 MeV impinges on a target of CmO_2. At this energy, the $^{296}116$ is produced in a very excited state that decays in $\sim 10^{-21}$ s by neutron emission

$$^{296}116 \rightarrow {}^{292}116\ 4\mathrm{n}\ . \tag{2.68}$$

The target is sufficiently thin that the $^{292}116$ emerges from the target with most of its energy.

Only about 1 in 10^{12} collisions result in the production of element 116, most inelastic collisions resulting in the fission of the target and beam nuclei. It is therefore necessary to place beyond the target a series of magnetic and electrostatic filters so that only rare super-heavy elements reach a silicon-detector array downstream.

The $^{292}116$ ions then stop in the silicon-detector array where they eventually decay. The three sequences of events shown in Fig. 2.20 have been observed. The three sequences are believed to be due to the same nuclide because of the equality, within experimental errors, of the Q_α. The lifetimes for each step are also of the same order-of magnitude so the half-lives can be estimated. The use of (2.61) then allows one to deduce the (A, Z) of the nuclei, confirming the identity of element 116.

Efforts to produce of super-heavy elements are being vigorously pursued. They are in part inspired by the prediction of some shell models to have an island of highly-bound nuclei around $N \sim 184$, $Z \sim 120$. There are speculations that elements in this region may be sufficiently long-lived to have practical applications.

2.9 Bibliography

1. *Nuclear Structure* A. Bohr and B. Mottelson, Benjamin, New York, 1969.
2. *Structure of the Nucleus* M.A. Preston and R.K. Bhaduri, Addison-Wesley, 1975.
3. *Nuclear Physics* S.M. Wong, John Wiley, New York, 1998.
4. *Theoretical Nuclear Physics* A. de Shalit and H. Feshbach, Wiley, New York, 1974.
5. *Introduction to Nuclear Physics* : Harald Enge, Addison-Wesley (1966).

Exercises

2.1 Use the semi-empirical mass formula to calculate the energy of α particles emitted by $^{235}U_{92}$. Compare this with the experimental value, 4.52 MeV. Note that while an α-particles are unbound in ^{235}U individual nucleons are bound. Calculate the energy required to remove a proton or a neutron from ^{235}U.

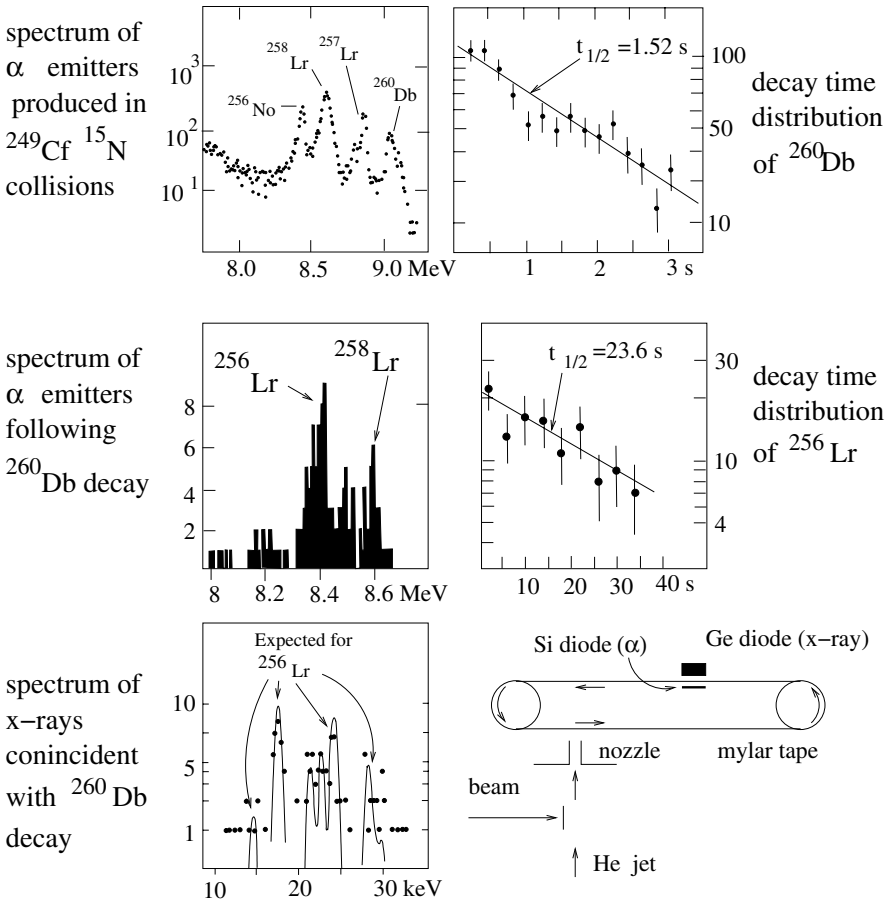

Fig. 2.19. The production and identification of element 105 ^{260}Db via the reaction $^{249}\mathrm{Cf}(^{15}\mathrm{N}, 4\mathrm{n})^{260}\mathrm{Db}$ [28]. As shown schematically on the bottom right, a beam of 85 MeV ^{15}N nuclei (Oak Ridge Isochronous Cyclotron) is incident on a thin ($635\,\mu\mathrm{g\,cm^{-2}}$) target of ^{249}Cf ($Cf_2O_3$) deposited on a beryllium foil ($2.35\,\mathrm{mg\,cm^{-2}}$). Nuclei emerging from the target are swept by a helium jet through a nozzle where they are deposited on a mylar tape. After a deposition period of ~ 1 s, the tape is moved so that the deposited nuclei are placed between two counters, a silicon diode to count α-particles and a germanium diode to count x-rays. The α-spectrum (upper left) shows three previously well-studied nuclides as well has that of ^{260}Db at ~ 9.1 MeV. The top right panel shows the distribution of decay times indicating $t_{1/2} = 1.52 \pm 0.13$s. Confirmation of the identity of ^{260}Db comes from the α-spectrum for decays following the the 9.1 MeV α-decays. The energy spectrum indicates that the following decay is that of the previously well-studied ^{256}Lr. (The small amount of ^{258}Lr is due to accidental coincidences. Finally, the chemical identity of the Lr is confirmed by the spectrum of x-rays following the *atomic* de-excitation. (The Lr is generally left in an excited state after the decay of ^{260}Db.)

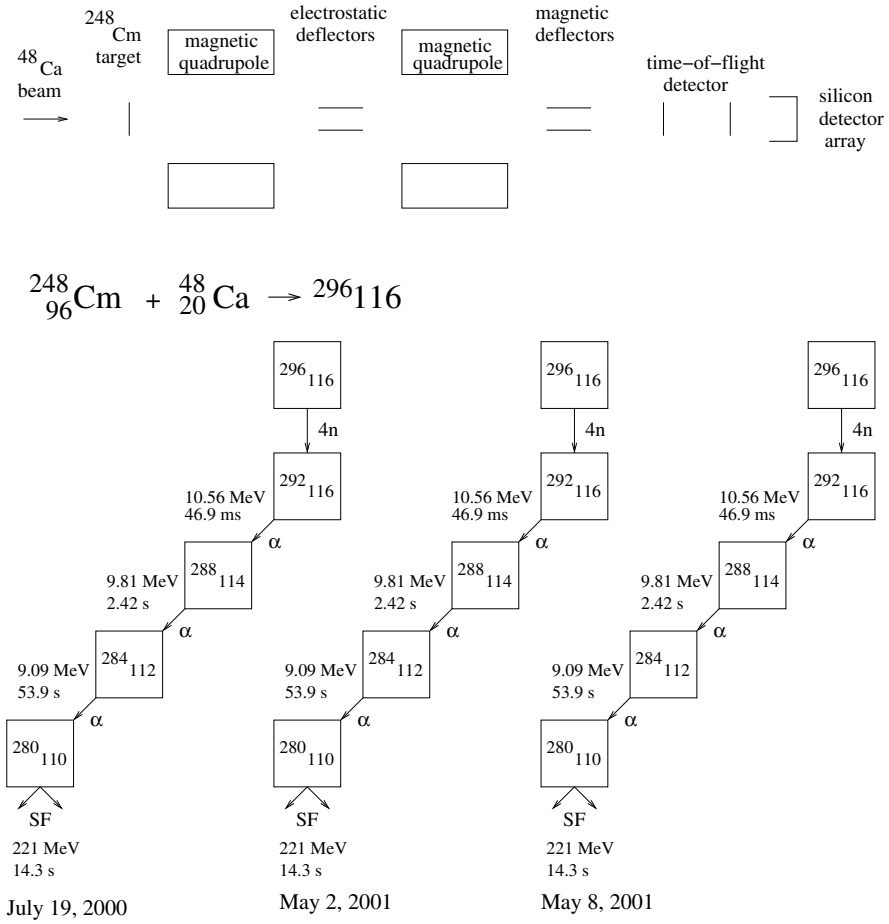

Fig. 2.20. The production of element 116 in ^{48}Ca-^{248}Cm collisions. The top panel shows the apparatus used by [29]. Inelastic collisions generally produce light fission nuclei. Super-heavy nuclei are separated from these light nuclei by a system of magnetic and electrostatic deflectors and focusing elements. Nuclei that pass through this system stop in a silicon detector array (Chap. 5) that measures the time, position and deposited energy of the nucleus. Subsequent decays are then recorded and the decay energies measured by the energy deposited in the silicon. The bottom panel shows 3 observed event sequences that were ascribed in [29] to production and decay of ^{296}116. The three sequences all have 3 α decays whose energies and decay times are consistent with the hypothesis that the three sequences are identical.

2.2 The radius of a nucleus is $R \simeq r_0 A^{1/3}$ with $r_0 = 1.2$ fm. Using Heisenberg's relations, estimate the mean kinetic momentum and energy of a nucleon inside a nucleus.

2.3 Consider the nucleon-nucleon interaction, and take the model $V(r) = (1/2)\mu\omega^2 r^2 - V_0$ for the potential. Estimate the values of the parameters ω and V_0 that reproduce the size and binding energy of the deuteron. We recall that the wave function of the ground state of the harmonic oscillator is $\psi(r, \theta, \phi) \propto \exp(-m\omega r^2/2\hbar)$. Is a $\ell = 1$ state bound predicted by this model?

2.4 Consider a three-dimensional harmonic oscillator, $V(r) = (1/2)m\omega^2 r^2$. the energy eigenvalues are

$$E_n \;=\; (n + 3/2)\hbar\omega \qquad n \;=\; n_x + n_y + n_z \;, \tag{2.69}$$

where $n_{x,y,z}$ are the quantum numbers for the three orthogonal directions and can take on positive semi-definite integers. We denote the corresponding eigenstates as $|n_x, n_y, n_z\rangle$. They satisfy

$$x|n_x, n_y, n_z\rangle \;=\; \frac{\sqrt{n_x - 1}}{\alpha}|n_x - 1, n_y, n_z\rangle \;+\; \frac{\sqrt{n_x + 1}}{\alpha}|n_x + 1, n_y, n_z\rangle \;,$$

and

$$\mathrm{i}p|n_x, n_y, n_z\rangle \;=\; \frac{\sqrt{n_x - 1}}{\alpha}|n_x - 1, n_y, n_z\rangle \;-\; \frac{\sqrt{n_x + 1}}{\alpha}|n_x + 1, n_y, n_z\rangle \;,$$

where $\alpha = \sqrt{2m\omega/\hbar}$. Corresponding relations hold for y and z. These states are not generally eigenstates of angular momentum but such states can be constructed from the $|n_x, n_y, n_z\rangle$. For example, verify explicitly that the $E = (1/2)\hbar\omega$ and $E = (3/2)\hbar\omega$ states can be combined to form $l = 0$ and $l = 1$ states:

$$|E = (1/2)\hbar\omega, l = 0, l_z = 0\rangle \;=\; |0, 0, 0\rangle \;,$$

$$|E = (3/2)\hbar\omega, l = 1, l_z = 0\rangle \;=\; |1, 0, 0\rangle \;,$$

$$|E = (3/2)\hbar\omega, l = 1, l_z = \pm 1\rangle \;=\; (1/\sqrt{2})\left(|0, 1, 0\rangle \pm \mathrm{i}|0, 0, 1\rangle\right) \;.$$

2.5 Verify equations (2.40).

2.6 Use Fig. 2.10 to predict the spin and parity of ^{41}Ca.

2.7 The nuclear shell model makes predictions for the magnetic moment of a nucleus as a function of the orbital quantum numbers. Consider a nucleus

consisting of a single unpaired nucleon in addition to a certain number of paired nucleons. The nuclear angular momentum is the sum of the spin and orbital angular momentum of the unpaired nucleon:

$$\boldsymbol{J} \;=\; \boldsymbol{S} \,+\, \boldsymbol{L}\,. \tag{2.70}$$

The total angular momentum (the nuclear spin) is $j = l \pm 1/2$ for the nucleon spin aligned or anti-aligned with the nucleon orbital angular momentum. The two types of angular momentum do not contribute in the same way to the magnetic moment:

$$\boldsymbol{\mu} \;=\; g_l \frac{e\boldsymbol{L}}{2m} \;+\; g_s \frac{e\boldsymbol{S}}{2m} \tag{2.71}$$

where $m \sim m_{\rm p} \sim m_{\rm n}$ is the nucleon mass, $g_l = 1$ ($g_l = 0$) for an unpaired proton (neutron) and $g_s = 2.792 \times 2$ ($g_s = -1.913 \times 2$) for a proton (neutron). The ratio between the magnetic moment and the spin of a nucleus is the *gyromagnetic ratio*, g. It can be defined as

$$g \;\equiv\; \frac{\boldsymbol{\mu} \cdot \boldsymbol{J}}{\boldsymbol{J} \cdot \boldsymbol{J}} \tag{2.72}$$

Use (2.40) to show that

$$g \;=\; (j - 1/2)g_l + (1/2)g_s \qquad \text{for } l = j - 1/2 \tag{2.73}$$

$$g \;=\; \frac{j}{j+1}\left[(j + 3/2)g_l - (1/2)g_s\right] \qquad \text{for } l = j + 1/2\,. \tag{2.74}$$

Plot these two values as a function of j for nuclei with one unpaired neutron and for nuclei with one unpaired proton. Nuclei with one unpaired nucleon generally have magnetic moments that fall between these two values, known as the *Schmidt limits*.

Consider the two $(9/2)^+$ nuclides, ${}^{83}_{36}\mathrm{Kr}$ and ${}^{93}_{41}\mathrm{Nb}$. Which would you expect to have the larger magnetic moment?

2.8 Verify (2.59) by using

$$\lim_{u_{\rm min} \to 0} \int_{u_{\rm min}}^{1} \sqrt{u^{-1} - 1}\mathrm{d}u \;\sim\; \int_0^1 \sqrt{u^{-1} - 1}\mathrm{d}u \;-\; \int_0^{u_{\rm min}} \sqrt{u^{-1}}\mathrm{d}u\,.$$

2.9 To justify (2.55) write the wavefunction as

$$\psi(r) = C\exp(-\gamma(r)) + D\exp(+\gamma(r)) \quad . \tag{2.75}$$

In the WKB approximation, we suppose that $\psi(r)$ varies sufficiently slowly that we can neglect $(\mathrm{d}^2/\mathrm{d}r^2)\gamma(r) \sim 0$. In this approximation, show that

$$\frac{\mathrm{d}^2\psi}{\mathrm{d}r^2} \sim \left(\frac{\mathrm{d}\gamma}{\mathrm{d}r}\right)^2 \psi \tag{2.76}$$

and that the Schrödinger becomes

$$(\frac{\mathrm{d}\gamma}{\mathrm{d}r})^2 \psi + \frac{2M}{\hbar^2}(E - \frac{2Ze^2}{4\pi\epsilon_0 r})\psi = 0 \ , \tag{2.77}$$

i.e.

$$(\frac{\mathrm{d}\gamma}{\mathrm{d}r}) = \sqrt{\frac{2M}{\hbar^2}(E - \frac{2Ze^2}{4\pi\epsilon_0 r})} \quad , \tag{2.78}$$

which is the desired result.

Springer

http://www.springer.com/978-0-387-01672-6

Fundamentals in Nuclear Physics
From Nuclear Structure to Cosmology

Basdevant, J.-L.; Rich, J.; Spiro, M.

2005, XIV, 516 p. 184 illus., Hardcover
ISBN: 978-0-387-01672-6